Treball Final del Grau

Enginyeria Fisica

Development of a multihit LADAR imaging camera system:

Modelling Time of Flight under diffusion conditions

Marc Far Ruiz

Dirigit per:

Santiago Royo Royo

Universitat Politècnica de Catalunya

Juny 2016

Abstract

Time-Of-Flight (or Lidar, or Ladar) imaging is a very common technique to obtain 3D images, giving information about the time of the pulse and its energy. However, in turbid media, such as the ocean or with the presence of fog, TOF method doesn't give neither a correct radiometric information nor of its raytrace. The reason is that the images obtained are strongly blurred, due to their strong scattering condition, which make the rays change many times their direction.

The impending creation of a 3D LIDAR imaging camera, in the Centre of Sensors, Instruments and Systems Development (CD6), that works in these type of media requires the presence of a more accurate model that keeps diffusion in mind and has a temporal dependence.

This model is called the "Diffusion Model" which is a simple, but valid approximation for scattering media in the Lidar case. Such a model doesn't have the spatial resolution that other methods such as Monte Carlo or Finite Elements can give, but can provide information about the temporal dependence of the photon transport with a simple approach. It also separates the effects of scattering and absorption, providing a more accurate approximation compared to Beer's law, which doesn't separate both effects and takes them as one, the attenuation.

The goal of this project is to develop and validate this Diffusion Model, which has a temporal dependence and could be valid in strong scattering conditions, simulating the ones that are common in the ocean in order to provide help to the development of the LADAR imaging camera system in CD6, Terrassa.

Acknowledgements

Contents

List of figures

Chapter 1

Introduction

After more than 40 years of its invention, the LIDAR (Laser Imaging Detector and Ranging) has become an important tool for the measurement of distances. The fact that its divergence is two or three magnitude orders less than the one of a conventional RADAR makes LIDAR systems have a high spatial resolution. Therefore, it is very useful for certain applications related with mapping.

Lately there has been an increment on the interest in LIDAR systems, as a complement to conventional image systems based on 2D images. Self-guided vehicles or navigation support systems require new sensors which allow the detection of images in real time [1]. Moreover, there's a need of a higher resolution systems for 3D imaging, that encourages the research and implementation of these LIDAR systems.

One type of LIDAR camera is the Time-of-flight camera (ToF camera) in which the entire scene is captured measuring distance using the phase of a modulated RF wave, as opposed to point-by-point measurements with a laser beam such as in scanning LIDAR systems. In these systems, the laser beam is reflected by the different objects, such as buildings or cars. Once the return pulses have been registered, the distance between the sensor and the objects can be calculated, by knowing the speed of light and the time it took to the light to travel to the object and back to the sensor, giving its name to a camera.

Time-Of-Flight imaging is a very common technique to obtain 3D images, giving information about the time of the pulse and its energy. However, in turbid media, such as the ocean or with the presence of fog, TOF method doesn't give neither a correct radiometric information nor a proper time dependence, as its raytrace is not anymore useful. The impending creation of a 3D LIDAR imaging camera working in these type of media requires the presence of a more accurate model that keeps diffusion in mind and has a temporal dependence.

In turbid media, such as the ocean, the images obtained are strongly blurred, due to their strong scattering condition, which make the rays change many times their direction.

In the direct detection of objects in subaquatic media, there are nowadays theoretical models that explain its performance and many simulations, but with idealized conditions and neglecting relevant effects such as multiple scattering. There are also theoretical models that explain how the LIDAR works in the ocean. [2]

However, the propagation conditions of the light pulses in multiple scattering conditions are known and well defined in the tissue optics field. Hence, a simulation applying this scattering condition could be possible.

The main goal of this project is to develop and validate a new method that has a temporal dependence and could be valid in strong scattering conditions, simulating the ones that are common in the ocean. This simulation might help to the development of a multihit Lidar camera system, which is already under construction in CD6 (Centre for Sensors, Instruments and Systems Development)[3]

Once the model is studied and analysed, we want to make a simulation of the light transport in this strong scattering conditions, and see its behaviour. One of the main aspects of these conditions is the presence of a delay in the time measure, with respect to the original TOF time t=2d/v. In this project we want to quantify this delay and make a relation between the measured distances and their real values for different scattering conditions.

In the project report, first we will talk about the properties of the scattering media, then we will explain in detail the conventional scattering models, such as Mie or Rayleigh. After that, different models that can be applied under diffusion conditions are explained and compared. A little overview of the Lidar Equation and the specific properties of sea water are explained before the explanation and results of the simulation.

Chapter 2

Theoretical Background

2.1. Propagation on Scattering Media

2.1.1. Scattering Media

Scattering media, as the name itself indicates, is any medium where the scattering is the most important event. In any medium, there are two events: scattering and absorption. So, in scattering media several scattering events take place before an absorption one.

In this chapter a brief explanation of scattering and absorption is made, as well as the definition of another important factor in scattering media, which is the anisotropy factor.

2.1.1.1. Scattering

Scattering of the light may be thought as the redirection of light when an electromagnetic wave encounters an obstacle or non-homogeneity, such as a scattering particle. It is weakly spectrally dependent.
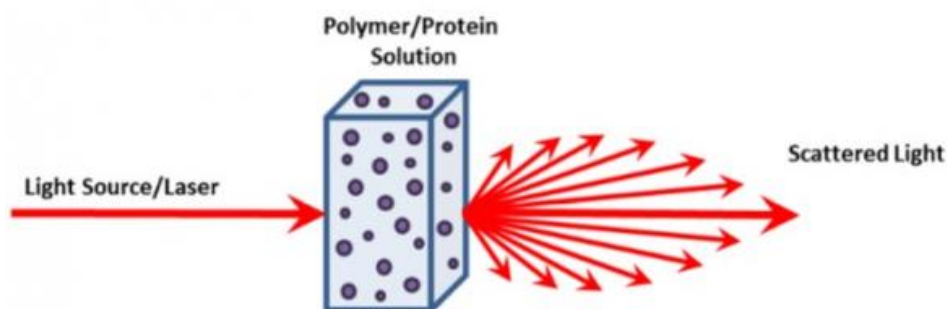
Figure 1. Example of light scattering.

There are two types of scattering: elastic and inelastic.

- Elastic scattering, where the kinetic energy of the photon is conserved in the center-of-mass frame, but its direction of propagation is modified. Hence, generally, the total kinetic energy of the system is conserved.

- Inelastic scattering, where the kinetic energy of the incident photon is not conserved, because some of its energy is lost or increased.

  One example of inelastic scattering is called the Raman scattering, which is the scattering of a photon upon interaction with matter. It only occurs with a small fraction of the scattered photons (about 1 in 10 million).

As the inelastic scattering is less common, we will focus on the different types of elastic scattering. It will depend on the particle size and may be λ-dependent.

In order to classify the different types of elastic scattering, a dimensionless size parameter *a* is defined, which is:

$$\alpha = {2\pi r}/{\lambda} \qquad (1)$$

where r is the characteristic length (radius) of the particle and λ is the wavelength of incident radiation. Depending on the value of α, a certain type of scattering will occur.

When α << 1, which means that the size of the particle is small compared with the wavelength, the type of scattering will be "Rayleigh Scattering"

When $\alpha \sim 1$, the particle has the same size as the wavelength of the light. It occurs the "Mie Scattering"

When α >> 1, the particle is larger than the wavelength of the light. In this situation, the "geometric scattering" takes place. Sometimes is also called "Mie Scattering".
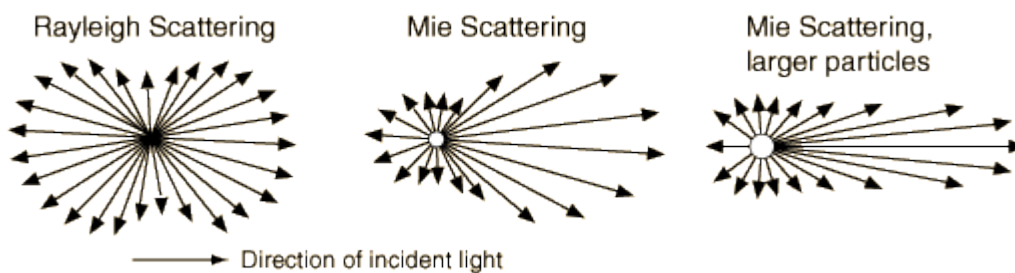
Figure 2. Differences between Rayleigh, Mie and Geometry scattering

We also have to differentiate between single and multiple scattering. In single scattering, as its name says, only one single scattering event takes place. It occurs when $\mu_s L \ll 1$ and the coherence, the phase, the polarization and the raytrace could be preserved. On the other hand, in multiple scattering no coherence, no phase, no polarization and no raytrace can be preserved. Several scattering events take place at the same time and it occurs when $\mu_s L \gg 1$.

2.1.1.2. Absorption

Absorption is the reason why the photons permanently remove from the path and it is highly spectrally dependent. It is usually expressed as a function of the wavelength: $\mu_a(\lambda)[\,\mathrm{m}^{-1}]$.

Absorption, as an inherent optical property, can be decomposed into groups with certain similarity. These groups are: absorption due to water $\mu_{a,w}(\lambda)$, phytoplankton $\mu_{a,phyt}(\lambda)$, non-algal particles $\mu_{a,NAP}(\lambda)$, and colored dissolved organic matter $\mu_{a,CDOM}(\lambda)$.[4]

$$\mu_a(\lambda) = \mu_{a,w}(\lambda) + \mu_{a,phyt}(\lambda) + \mu_{a,NAP}(\lambda) + \mu_{a,CDOM}(\lambda) \qquad (2)$$

2.1.1.3. Anisotropy Factor

The anisotropy factor, g, is dimensionless and it is the average cosine of the scattering angle θ: $g \equiv \int_{4\pi} f(\hat{\Omega} \cdot \hat{\Omega}')\hat{\Omega} \cdot \hat{\Omega}' d\hat{\Omega} = <cos\theta>$, where $f(\hat{\Omega} \cdot \hat{\Omega}')$ is the normalized differential cross-section for single light scattering events and gives the probability that light is scattered into the direction $\hat{\Omega}'$, knowing that its incident direction was $\hat{\Omega}$.

2.1.2.   Conventional scattering Models

As explained in the "Scattering media" chapter, depending on the size of the scattering particle a certain type of scattering event will take place. In this chapter we will discuss the two most important scattering models: The Mie theory and the Rayleigh Theory.

2.1.2.1.   Rayleigh Theory

Rayleigh scattering is the elastic scattering of light by particles much smaller than the wavelength of the radiation and it results from the electric polarizability of the particles. In the Rayleigh scattering the whole surface re-radiates with the same phase.

In this model, the scattering light is incoherent and the resulting intensity is the sum of the squares of each particle amplitude. Hence, this intensity is proportional to the sixth power of the size of the particle and to the inverse fourth power of the wavelength.[5]

Giving this intensity in detail, it is:

$$I = I_0 \frac{1 + cos^2\theta}{2R^2} \left(\frac{2\pi}{\lambda}\right)^4 \left(\frac{n^2 - 1}{n^2 + 2}\right)^2 r^6 \qquad (3)$$

Where I_0 is the intensity of the unpolarized light, λ its wavelength, θ the scattering angle, n the refractive index, r the characteristic length of the particle (radius) and R the distance to the particle.

By averaging equation (3) over all the angles, we have the Rayleigh scattering cross-section:

$$\sigma_s = \frac{2\pi^5}{3} \frac{d^6}{\lambda^4} \left(\frac{n^2 - 1}{n^2 + 2}\right)^2 \qquad (4)$$

With d=2r, the diameter of the particle.

Logically, the scattering cross-section is also proportional to the sixth power of the size of the particle and to the inverse fourth power of the wavelength. This dependence is the reason of the blue colour of the sky, as the molecules that are present in the air, like O_2

and N$_2$ are relatively small and fulfil the conditions of the Rayleigh model. The strong wavelength dependence of the scattering means that shorter wavelengths, as the blue ones, are more redirected out of the direct path to all directions as scattered light than the longer wavelengths (red).

It is the preferred theory if applicable, due to the complexity of the Mie Theory explained below.

2.1.2.2.   Mie Theory

Rayleigh scattering is the elastic scattering of light by a homogeneous sphere of approximately the same size as the wavelength of the incident light. The solution takes the form of an infinite series of spherical multipole partial waves.

In this case a new parameter is defined, the differential scattering cross section for unpolarized incident light, which is [6]:

$$\sigma'_{scat} = \frac{\lambda^2}{8\pi^2}(i_1 + i_2) \tag{5}$$

With i_1 and i_2 angular intensity functions of the following form:

$$i_1 = \left| \sum_{n=1}^{\infty} \frac{2n+1}{n(n+1)} [a_n \pi_n(cos\theta) + b_n \tau_n(cos\theta)] \right|^2 \tag{6}$$

$$i_2 = \left| \sum_{n=1}^{\infty} \frac{2n+1}{n(n+1)} [a_n \tau_n(cos\theta) + b_n \pi_n(cos\theta)] \right|^2 \tag{7}$$

Where the parameters a_n and b_n are defined as:

$$a_n = \frac{\psi_n(\alpha)\psi'_n(m\alpha) - m\psi_n(m\alpha)\psi'_n(\alpha)}{\xi_n(\alpha)\psi'_n(m\alpha) - m\psi_n(m\alpha)\xi'_n(\alpha)} \tag{8}$$

$$b_n = \frac{m\psi_n(\alpha)\psi'_n(m\alpha) - \psi_n(m\alpha)\psi'_n(\alpha)}{m\xi_n(\alpha)\psi'_n(m\alpha) - \psi_n(m\alpha)\xi'_n(\alpha)} \tag{9}$$

And m is the complex refractive index: $m = n - ik$ and ψ and ξ are called Ricatti-Bessel functions:

$$\psi_n(z) = \left(\frac{\pi z}{2}\right)^{\frac{1}{2}} J_{n+1/2}(z),$$

(10)

$$\xi_n(z) = \left(\frac{\pi z}{2}\right)^{\frac{1}{2}} H_{n+1/2}(z)$$

(11)

In equation (10), $J_{n+1/2}(z)$ is the half-integer-order Bessel function of the first kind, while in equation (11), $H_{n+1/2}(z)$ is the half-integer-order Hankel function of the second kind.

With all these terms, the definition of the Mie scattering cross-section is made, which is:

$$\sigma_{scat} = \frac{\lambda^2}{2\pi} \sum_{n=0}^{\infty} (2n + 1)(|a_n|^2 + |b_n|^2)$$

(12)

It is a model much more difficult to implement than the Rayleigh model, that's why it is preferred to use the Rayleigh approximation when it could be applicable.

2.1.3   The Diffusion Model

Light propagation in ocean water is mainly affected by scattering. It is also affected by absorption, but with less relevance. In order to separate the effects of both scattering and absorption, a new model is required, which is known as the diffusion model.

It starts from the transport theory and it focuses mainly in the light radiance L $(r,\hat{\Omega},t)$ [$\mathrm{W\ m^{-2} sr^{-1}}$], which is related to the light electric field E $(r,\hat{\Omega},t)$ by: $L \sim |E (r, \hat{\Omega}, t)|^2$. From this radiance and other IOPs (Inherent Optical Properties) one can derive an equation, the Radiation Transfer Equation (RTE), which relates how a medium affects a beam of light traveling through it. The loss of radiance depends basically on the absorption and scattering coefficients. The absorption coefficient is called μ_a and the scattering one μ_s. Both are expressed in units of $\mathrm{m^{-1}}$.

In order to make the equation easier to solve, several approximations were made. Firstly, L is written as a series expansion of spherical harmonics truncated at l=N (P$_N$ approximation). [7]

If L $(r,\hat{\Omega},t)$ is nearly isotropic (meaning that it doesn't change with the direction you are measuring to) this series is truncated at N=1 (P$_1$ approximation), giving a simpler equation [8]:

$$L\left(r,\hat{\Omega},t\right) = \frac{1}{4\pi}\Phi(r,t) + \frac{3}{4\pi}J(r,t)\cdot\hat{\Omega} \tag{13}$$

In this equation two new quantities appear, the photon flux $J(r,\ t)$ [W m^{-2}], and the photon fluence rate $\Phi(r,\ t)$ [W m^{-2}], which we used the most.

$J(r,t)\cdot\hat{\Omega}$ gives the power per area travelling in the solid angle $\hat{\Omega}$ direction at position r and time t.

We can relate these two new quantities with a continuity equation:

$$\frac{1}{v}\frac{\partial\,\Phi(r,t)}{\partial t} + \nabla\cdot J(r,t) + \mu_a\,\Phi(r,t) = S(r,t) \tag{14}$$

With $S(r,\ t)$ [W cm^{-3}] is the total power per volume emitted radially outward.

The relation between the photon fluence rate and its flux in the P$_1$ approximation is given by:

$$\nabla\Phi(r,t) = -\frac{3}{v}\frac{\partial\,J(r,t)}{\partial t} - 3\mu_t\,J(r,t) + 3\int Q\left(r,\hat{\Omega},t\right)\hat{\Omega}\,d\Omega + 3\mu_s g\,J(r,t) \tag{15}$$

where μ_t is the total attenuation coefficient: $\mu_t = \mu_a + \mu_s$, and g is the anisotropy factor which is defined by the average cosine of the scattering angle θ: $g \equiv <cos\theta>$. This factor goes from 0 to 1 and the closer it is to one, the more probable a photon will be scattered forwardly.

However, the P$_1$ approximation is due to nearly-isotropic conditions, so $Q\left(r,\hat{\Omega},t\right) = Q(r,t)$ and its integral in equation **(15)** is zero.

Assuming also slow temporal variations in the flux J (r, t) then the term $\frac{1}{v}\frac{\partial J(r,t)}{\partial t}$ in equation (15) is so small compared to $(\mu_t - \mu_s g) J(r, t)$ that can be neglected.

With these two approximations, equation (15) becomes simpler:

$$\nabla \Phi(r, t) = -3\mu_t J(r, t) + 3\mu_s g\, J(r, t) = -3(\mu_t - \mu_s g)J(r, t) \qquad (16)$$

Remembering that $\mu_t = \mu_a + \mu_s$ and simplifying the equation (16) we have:

$$\nabla \Phi(r, t) = -3(\mu_a + \mu_s(1 - g))J(r, t) \qquad (17)$$

The second term inside the parenthesis is defined as the reduced scattering coefficient: $\mu_s' \equiv \mu_s(1 - g)$.

Finally, equation (17) stays as:

$$\nabla \Phi(r, t) = -3(\mu_a + \mu_s') J(r, t) \qquad (18)$$

Replacing equation (18) into equation (14) we have the photon diffusion equation for the photon fluence rate:

$$\nabla \cdot \left(D(r)\nabla \Phi(r, t)\right) - v\mu_a \Phi(r, t) - \frac{\partial \Phi(r, t)}{\partial t} = -vS(r, t) \qquad (19)$$

As the name of the model states, diffusion has an important relevance in the behavior of the light, so its presence in this model is obvious. That's why we define the photon diffusion coefficient $D(r) = \frac{v}{3\,(\mu_s'(r) + \mu_a(r))}$.

But when can we apply the photon diffusion model? Its validity rests on the validity of the P₁ approximation. This means that the radiance needs to be almost isotropic. This isotropy is achieved when scattering is much greater than absorption. As a general rule, in order to apply correctly the photon diffusion model, the coefficient μ_s'/μ_a must be greater than 10.[9]

There are three types of light sources that are employed. These are: continuous wave (CW), intensity modulated (FD) and time pulsed. Each one has its advantages and disadvantages. Starting with the simpler one, the continuous wave, where the intensity remains constant at every time t. It allows the use of simple detector, but the absorption coefficient and the photon diffusion one can't be determined simultaneously. In intensity modulated sources, the light intensity is sinusoidally modulated. The resulting diffusive wave oscillates at the same frequency. With the phase measured between the input and the output, μ_a and D can be determined at the same time.

Finally, the type of source used in this bachelor thesis, the time pulsed light, which is related with the intensity modulated light explained above by means of a Fourier transform. This source emits a short light pulse, typically less than 100ps long[10]. As we will see later on in this project, the pulse temporally broadens as it propagates through the medium.
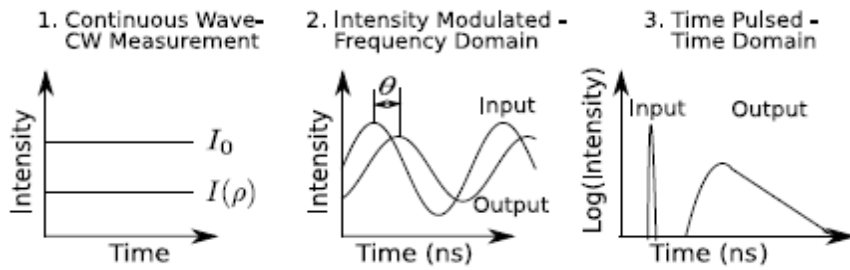
Figure 3. Emitted and detected light intensity for: 1) Continuous wave (CW), 2) Intensity Modulated (FD) and 3) Time Pulsed (TD)

We also assume that the source term has dc and ac parts, and can be written as: $S(r,t) = S_{dc}(r) + S_{ac}(r)e^{-i\omega t}$, with solutions of the ac part $\Phi_{ac}(r,t) = U(r)e^{-i\omega t}$

Replacing the ac solutions into the diffusion equation for the fluence rate (equation **(19)**) and considering homogeneous media, U(r) is described by:

$$(\nabla^2 - k^2)U(r) = -\frac{v}{D}S_{ac}(r) \qquad (20)$$

We will consider sea water as an infinite, homogeneous turbid media, as it is the simplest geometry to consider. Hence, the solution to equation **(20)** has the form of a simple overdamped spherical wave [11]:

$$U(r) = \frac{vS_{ac}}{4\pi Dr} \exp(-kr) \tag{21}$$

k is a complex wavevector $k = k_r + ik_i$ with:

$$k_r = \left(\frac{v\mu_a}{2D}\right)^{1/2} \left[\left(1 + \left[\frac{\omega}{v\mu_a}\right]^2\right)^{1/2} + 1\right]^{1/2} \tag{22}$$

$$k_i = -\left(\frac{v\mu_a}{2D}\right)^{1/2} \left[\left(1 + \left[\frac{\omega}{v\mu_a}\right]^2\right)^{1/2} - 1\right]^{1/2} \tag{23}$$

However we don't focus on the solution of equation **(21)**, because we need its Fourier transform, which gives us the fluence rate solution in the presence of a pulsed point source of the form $S(r,t) = S_0\delta(r)\delta(t)$.

So, the photon fluence rate in an infinite, homogeneous turbid media is given by:

$$\Phi(r,t) = \frac{vS_0}{(4\pi Dt)^{3/2}} \exp\left(-\frac{r^2}{4Dt} - \mu_a vt\right) \tag{24}$$

Having a quick look to the output intensity of a time pulsed source in Figure **3** we observe that for high values of t, the logarithm of the intensity decays as a straight line, with the slope being $-\mu_a v$. In other words, we can determinate the absorption coefficient because $\partial \ln \Phi(r,t) / \partial t$ tends to $-\mu_a v$ as $t \to \infty$. We will check it in another chapter later on.

2.1.4. Monte Carlo methods

Monte Carlo methods are different computational algorithms that rely on repeated random sampling to obtain numerical results. They have a broad range of applications, but most of them are related with physical or mathematical problems. In the physics field, these methods are specially used in problems with systems with many coupled degrees of freedom.

Monte Carlo methods are useful in order to solve problems that have probabilistic interpretations. One of the common applications is the approximate calculation of an integral by generating a large number of points randomly distributed and then calculating the number

of points inside the region of the desired integral, and making the ratio between them and the total points. By means of the law of large numbers, the value of the integral is well approximate with a large number of random points.

Another feature of the Monte Carlo method is that it also performs risk analysis, letting people see all the possible outcomes of their decisions and allowing for better decision making under uncertainty.

However, in this project, we will focus on the Monte Carlo Method for photon transport. In this case, the simulation is based on the random walks that photons make as they travel through the turbid media, usually tissue, but also applicable on water. These random walks are chosen by statistically sampling the probability distributions for step size and angular deflection per scattering event [12]. As explained before, in order to have an accurate approximation to reality and so considering the method valid, the number of propagating photons must be high.

The Diffusion model explained in the chapter before failed when the absorption was strong compared to scattering, but also failed when measuring distances too close to the source or to a boundary, so in these cases is when the Monte Carlo method steps in.

The Monte Carlo method is equivalent to modeling photon transport analytically by the radiative transfer equation (RTE), which describes the motion of photons using a differential equation, including all the processes that affect it, illustrated in Figure 4. However, it is easier to implement, as it is usually impossible to give a closed-form solution of the RTE.
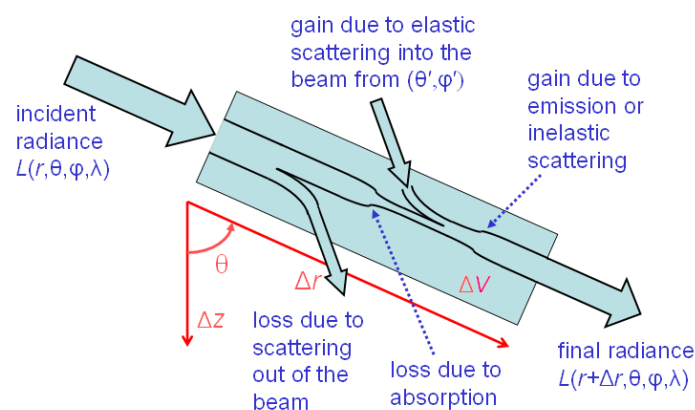
Figure 4. Illustration of the radiance and the processes that affect it as it propagates.

In order to apply the Monte Carlo method, both scattering and absorption coefficients as well as the anisotropy factor must be known. Its procedure is the following: First the photons must be generated in a specific location defined by *x, y* and *z* coordinates. Then the program takes the first photon and defines its step size Δs, being relatively small compared with the total mean free path of the photon [13]. This mean free path is, as explained before, the reciprocal of the total attenuation coefficient. Hence, the mean free path is the reciprocal of the sum between the absorption and the scattering coefficients. It is important to choose a good step size, because if it is too small, the photon won't interact with the medium, causing the inefficiency of the method. On the other hand, choosing a step size too large won't fit the realistic values of the distance travelled by the photons. Another option to make the method more efficient is to consider a different step size for each photon step, following Beer's law as its probability function.

Once the step size is known, the direction of the movement is defined, by means of three direction cosines, which are specified by taking the cosine of the angle that the photon's direction makes with each axis (x, y and z). These cosines are specified by μ_x, μ_y and μ_z, respectively. So, for a photon placed initially in the position (*x, y, z*), the new position (*x', y', z'*) will be defined as:

$$x' = x + \mu_x \Delta s$$
$$y' = y + \mu_y \Delta s \qquad\qquad (25)$$
$$z' = z + \mu_z \Delta s$$

At the end of the step the photon can be either scattered, absorbed or also reflected or transmitted if the photon hit the boundary. The weight of the photon is also reduced by means of absorption. Once the first step is over, a new trajectory is specified and then it is moved a random distance. This process is repeated until the photon escapes from the medium or it is absorbed, recording its final position. The same process occurs with all the propagated photons and is explained in the flow chart given in Figure **5**.

One of the main issues of the Monte Carlo method is that it needs significant computation time to achieve precision. On the other hand, Monte Carlo simulations can obtain multiple physical quantities at the same time.
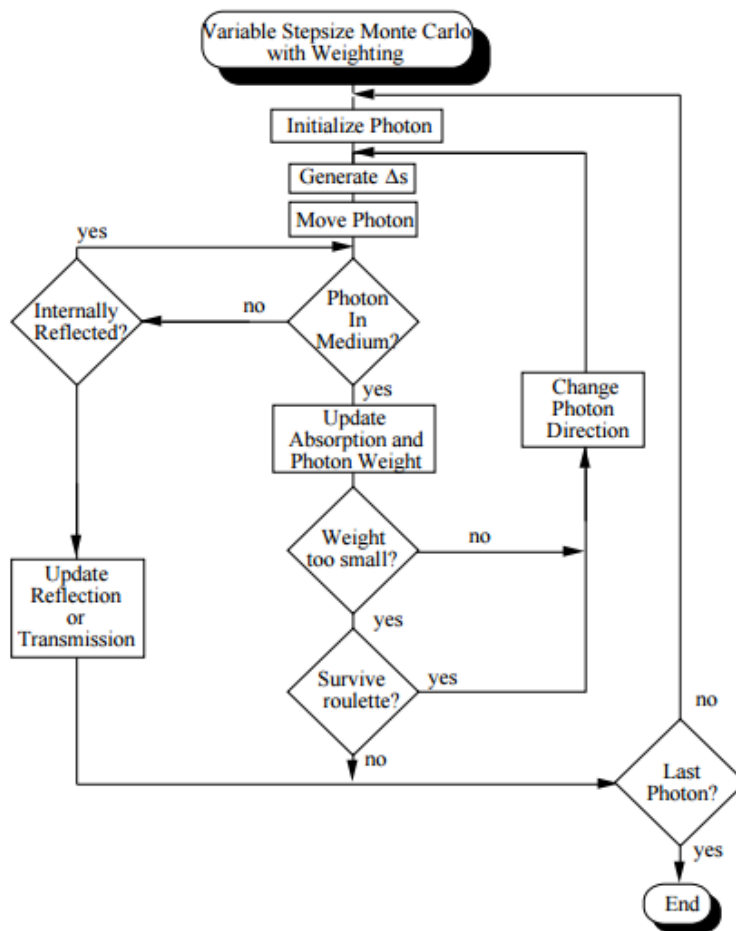
Figure 5. Flow chart of the variable Step size Monte Carlo method

Monte Carlo is a powerful tool to calculate the light transport with any desired spatial and temporal resolution, so it requires very intensive segmentation. It is especially useful when working in life sciences, when fine details and a large spatial resolution is involved. However, in the LIDAR camera this is not required. As in the ocean we are working in large distances and with big targets, we don't need much resolution. Therefore, we will work with the Diffusion Model, trying to bring an approximation to the photon transport and trying to compare its precision with the Monte Carlo method.

2.2.   Lidar: the range equation

Lidar equation is a quantitative approach to relate the received photon counts (light power) with several influence aspects, such as the emitted laser photon counts (laser power), light propagation, physical interaction between light and matter, geometry etc.

Its general form is:

$$N_S(\lambda, R) = N_L(\lambda_L) \cdot \left[\beta(\lambda, \lambda_L, \theta, R)\Delta R\right] \cdot \frac{A}{R^2} \cdot \left[T(\lambda_L, R)T(\lambda, R)\right] \cdot \left[\eta(\lambda, \lambda_L)G(R)\right] + N_B \quad (26)$$

Where: $N_S(R)$ is the expected received photon number from a distance R, N_L the number of transmitted laser photons, $\beta(R, \theta)$ the volume scatter coefficient at distance R for angle θ, ΔR the thickness of the range bin, A the area of the receiver, *T(R)* the one way transmission of the light, either from the laser source to the distance R or from distance R to the laser source; η the system optical efficiency, G(R) the geometrical factor of the system and, finally, N_B the background photon counts.

Therefore, the physical processes that are present in the Lidar Equation are: scattering (both elastic and inelastic), absorption, fluorescence, the Doppler effect (shift and broadening), the Boltzmann distribution and extinction.

The general equation form could be slightly modified, in order to obtain other equations, such as the LIDAR equation for arbitrary angle or for backscattering.

In the case of backscattering, the equation stays as:

$$N_S(\lambda, z) = \left(\frac{P_L(\lambda_L)\Delta t}{hc/\lambda_L}\right)(\beta(\lambda, \lambda_L, z)\Delta z)\left(\frac{A}{z^2}\right)(T(\lambda_L, z)T(\lambda, z))(\eta(\lambda, \lambda_L)G(z)) + N_B\Delta t \quad (27)$$

This equation can be divided into different terms:

The first term is $\left(\dfrac{P_L(\lambda_L)\Delta t}{hc/\lambda_L}\right)$, and is related with the transmitted photon number, which is the ratio between the transmitted laser energy within time bin and the energy of a single laser photon.

The second term, $(\beta(\lambda,\lambda_L,z)\Delta z)$ is the probability to be scattered. It is represented by the volume backscatter coefficient β, which is the probability that a photon is scattered at angle θ, using unitary magnitudes.

The third term is the probability to be collected by the receiving telescope, and is $\left(\dfrac{A}{z^2}\right)$.

The fourth part of the equation is the light transmission, where $\left(T(\lambda_L,z)T(\lambda,z)\right)$, is the atmospheric transmittance at outgoing wavelength λ_L and returning wavelength λ. This transmittance can be expressed as:

$$\left(T(\lambda_L,z)T(\lambda,z)\right) = exp\left[-\left(\int_0^R \alpha(\lambda_L,r)dr + \int_0^R \alpha(\lambda,r)dr\right)\right] \qquad (28)$$

With $\alpha(\lambda,r)$ the extinction coefficient.

Then it comes the overall system efficiency, $\left(\eta(\lambda,\lambda_L)G(z)\right)$, where $\eta(\lambda,\lambda_L)$ is the LIDAR hardware optical efficiency and G(z) is the geometrical form factor.

Finally, N_B are the background photon counts.

The General Lidar range equation is valid under two conditions: independent scattering and simple scattering. The first condition means that the particles have to be separated adequately and undergo random motion, which implies that the total scattered energy by the particles have no phase relation, being the total intensity only a sum of the intensity scattered from each particle. The single scattering condition is explained in the "Scattering Media" chapter, and states that each photon can be scattered only once. Hence, multiple scattering is not considered in the Lidar range equation.

We'll see later on that the usual regime in sea water is multiple scattering, so this General Lidar Range Equation can't be considered in our conditions, making it inappropriate to work with.

2.3. Sea Water

Sea water has certain differences from pure water, mostly due to the high number of dissolved and particulate matter, which vary significantly in kind and concentration. Hence, properties of sea water may have big spatial variations. In this chapter we will try to quantify the properties explained in the "Scattering Media" chapter, which are the scattering coefficient, the absorption coefficient and the anisotropy factor.

2.3.1. Scattering Coefficient

The values of the scattering coefficient differ greatly depending on the sea. And even in the same sea, it depends also on the depth in which you are measuring the coefficient, or the day among other factors. All these factors are the reason why the differences between the maximum scattering coefficient value and its minimum are huge. The range of values may go between 1 m^{-1} to 55 m^{-1} [14][15]. Although, in this project we will take only values that are valid in the diffusion model. This condition was explained in the "Diffusion Model" chapter, but its basis is the scattering dominance. Only high values of scattering are valid, since they have to fulfill $\mu_s(1 - g) > 10\mu_a$ [9], with μ_a the absorption coefficient and g the anisotropy factor explained below.

Moreover, in the case of the sea water, there are lots of dissolved and particulate matter of different size. Hence, there will be particles with size bigger, smaller and more or less equal than the wavelength of the light. This is the reason why the multiple scattering is the usual regime in the ocean.

2.3.2. Absorption

Depending on the type of sea water, the absorption will have different shapes. An example is introduced in Figure 6.
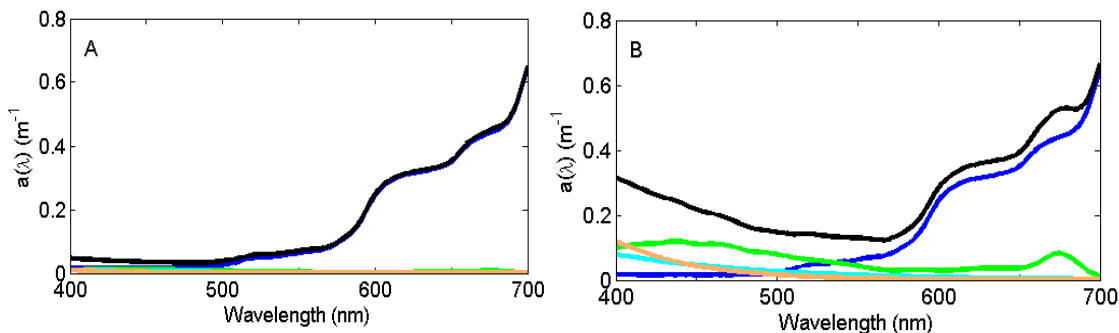
Figure 6. Examples of two absorption coefficient spectra in the visible range. The total absorption coefficient is represented in black; in blue, due to water; in green, due to phytoplankton; in light blue, due to non-algal particle and, finally, in brown due to colored dissolved organic matter. On the left there is an example of clear open sea water, where water dominates absorption and on the right there's a typical example of coastal water, where particulate and dissolved mater dominates absorption in short wavelengths, corresponding to blue and green spectrum. Picture taken from the Ocean Optics Web Book.

In our case, we consider the light source as a green light, so the wavelength will be 565nm. Following the example of this book, we will generally consider that $\mu_a(565) = 0.08\ m^{-1}$, but we will also take values between 0.05 and 0.2 for comparison [16][17][18].

2.3.3. Anisotropy factor

An accurate value of the factor hasn't been given yet, as it is extremely difficult to measure the factor. However, as a turbid media like the tissue, the typical value will be between 0.8 and 0.98 [19]. Depending of the type of water it will be a different value, with higher values corresponding to a higher number of photons scattered in the forward direction. In this project we will use by default g=0.9, but it can be changed sometimes specially in order to compare results.

This value of the anisotropy factor imposes that the reduced scattering coefficient $\mu'_s = \mu_s(1 - g) = 0.1\mu_s$. This means that if we want to fulfill the Diffusion model

condition, $\frac{0.1\mu_s}{\mu_a} > 10,$ which already means that the scattering coefficient has to be 100 times greater than the absorption coefficient.

Chapter 3

Results

In order to validate the diffusion model, a little simulation using MATLAB is prepared. A self-made code shows the features of this model.

In this chapter the results of the model are explained, divided into two subchapters. In the first one we will talk about the illumination on the target and in the second one, the features of the returned pulse will be discussed.

3.1. Illumination on the target: implementation and validation

In order to verify the shape of the photon fluence rate and its logarithm, we check it with a single point source, for Z=20m, g=0.9, $\mu_s = 8m^{-1}$ and $\mu_a = 0.08m^{-1}$. With these parameters, the Diffusion model condition is fulfilled. We plot the photon fluence rate of the central pixel and the corner pixel. The field of view of the target is 12.5x12.5m, which means that the corner pixel will be moved 6.25m in the x-axis and 6.25m in the y-axis. This is the result:
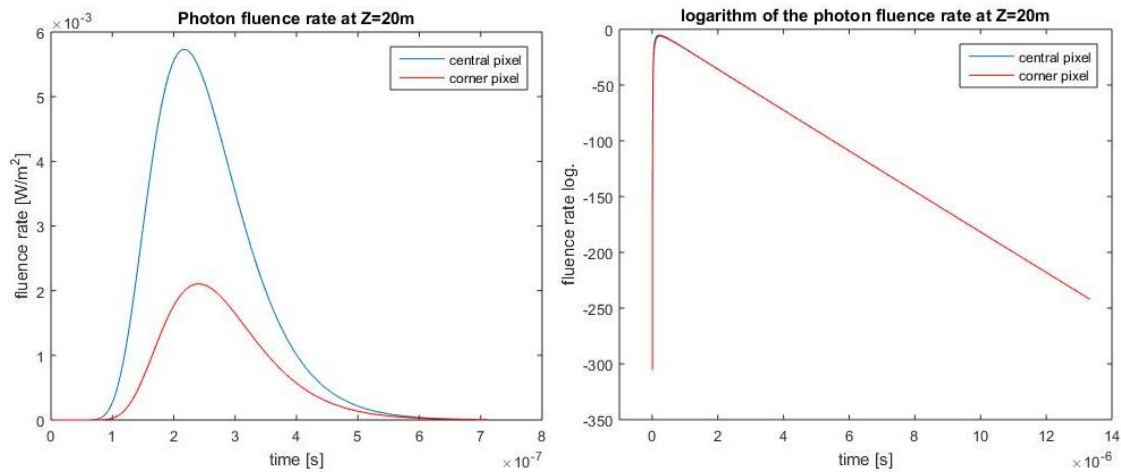
Figure 7. (a) Photon fluence rate at the central pixel (in blue) and in one of the corners (in red). (b) Logarithm of the fluence rate as a function of the time.

In Figure **7**(A), there are two main differences between the photon fluence rate in the central pixel and in the corner. The most significant difference is the value of the maximum, as it is almost three times greater in the centre. This difference is due to the big field of view we are using, which makes the distance much greater in the corner than in the centre. This difference in the distance is also the reason of the other difference, as the maximum of the corner takes place after the maximum in the central pixel.

Another property that has the fluence rate is the one explained at the end of the "Diffusion Model" Chapter: its logarithm decays as a straight line, with slope $-\mu_a v$, so we want to prove if our simulation fulfill the property, and its accuracy. In order to prove it, we set g=0.8 and $\mu_s = 12m^{-1}$ and, trying to be realistic with the values and also to fulfill the diffusion model condition, μ_a will go from $0.05m^{-1}$ to $0.12m^{-1}$.
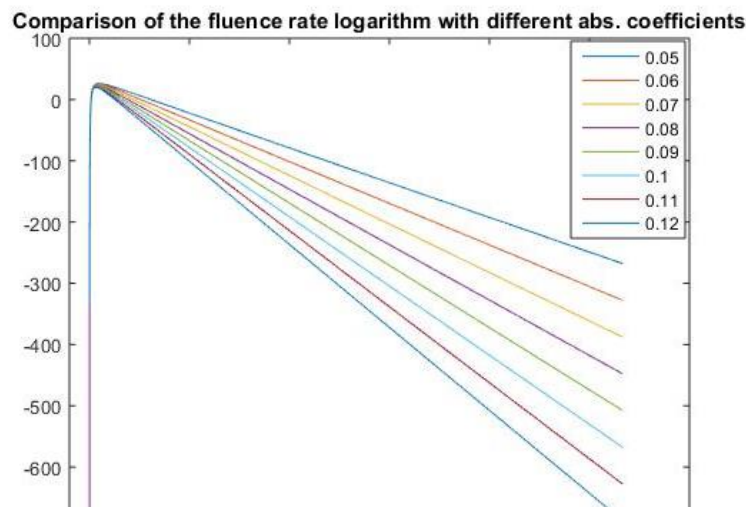
Figure 8. Comparison of the fluence rate logarithm with different absorption coefficients

The result is shown on the left in Figure **8**. At first sight, each logarithm behaves as a straight line at long times, and each one with different slope. The highest the absorption coefficient is, the highest the slope, which is coherent with the theory explained just above. However, this doesn't assure

the correct behavior of the simulation. Hence, we calculate the relative error of the absorption coefficient.

In order to calculate the slope, we make a very simple approximation: consider a period of time $dt = t_1 - t_0$ and make $f(t_1) - f(t_0)/dt$.

Trying with different dt periods from 100/v [s] to 1300/v [s] (with v=c/n), we have found that there's less error when the time period is low, although with a really small difference. It may be because at first sight the logarithm looks like a straight line, but if we look closer, the function would stabilize in the end.

We also want to compare the error given by different absorption coefficients, so the relative error is calculated, and plotted in Figure 9.
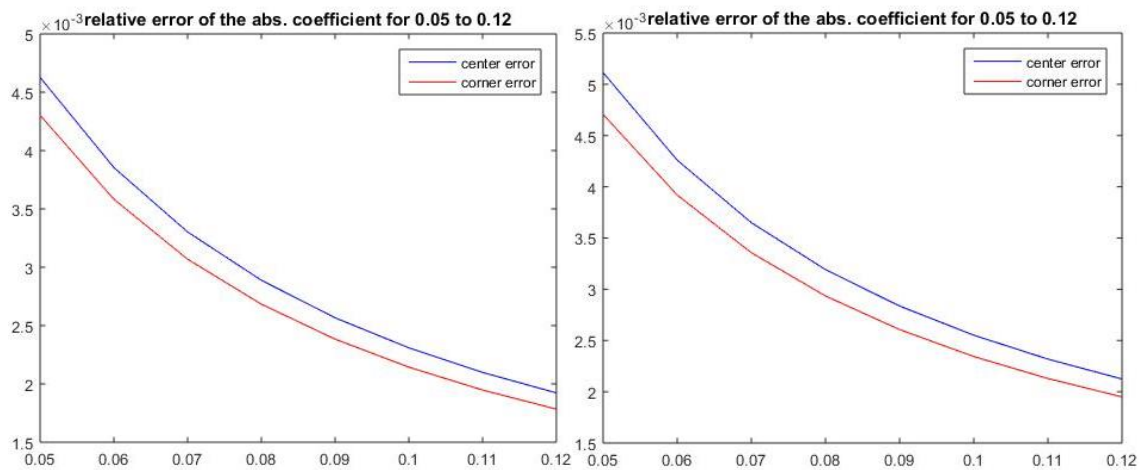
Figure 9. Relative error of the absorption coefficient calculated by means of the slope of the logarithm of the fluence rate. On the left, with dt=100/v and on the right, with dt= 1300/v

In the simulation, we calculate the fluence rate in the central pixel and in one of the corners, to see the difference. Therefore, the logarithm was also calculated and so was the slope. This is the reason why there are two different relative errors in the plots, one for the central pixel and one for the corner.

The first, and most evident result is that the relative error is really small, as it is always less than 0.5%. This could give us a way to calculate the absorption coefficient, although it would be difficult to implement. If a detector is able to show the fluence rate for every moment, with the help of a simple software that makes its logarithm, we can obtain the

coefficient. Another important result is that the greater the absorption coefficient, the lower the error.

Another important fact that happen is that by increasing the time interval of the measure, the error is a little bit less. However, if we increase too much the time period, the value of the absorption coefficient is infinite or Not A Number, probably due to logarithmic values too small or high that MATLAB can't handle. This situation is shown in Figure **10**, where we have achieved a reduction of the relative error in the lowest absorption coefficients, but there's a threshold value where the absorption coefficient can't be calculated, because the result is Not A Number.
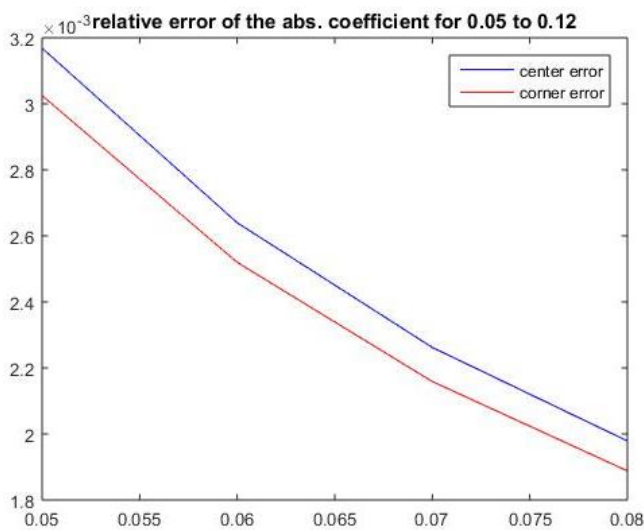
Figure 10. Relative error of the absorption coefficient calculated with a greater time period.

In this case, the time period in which we measure the photon fluence rate is 9000/v [s], instead of 6000/v [s] as in Figure **9**. As explained before, we have gained accuracy, because the relative error is a little bit lower, but MATLAB only calculated four values, until $\mu_a = 0.08 \, m^{-1}$. Hence, it is better to sacrifice accuracy in order to get more absorption values to calculate.

In our simulation, however, instead of having only one point source, we have discretized it by making a source set, like a 3x3 square lattice, respecting the beam divergence of a typical LIDAR system, which is 0.035°. Considering that the total energy in the light pulse is 0.001 J, and also assuming that the energy in the pulse of each source is uniform, each part of the source set will have an energy of 0.001/9 J

As we are working in scattering conditions, the introduction of delays is obvious. We want to measure this delay and describe how it varies when changing the scattering coefficient and make a relation between them. Another important point is to describe the variation of the time of the maximum fluence rate as a function of the distance of the target.

3.1.1. Variation in the scattering coefficient

Placing the target at a distance of Z=20m we want to see the features of the photon fluence rate with different scattering coefficients. In the "Diffusion Model" chapter the key condition in order to apply the model is explained in detail, but the reduced scattering coefficient needs to be at least ten times greater than the absorption coefficient. This reduced scattering coefficient was calculated by: $\mu'_s \equiv \mu_s(1-g)$.

In the "Sea Water" chapter we have said that the absorption coefficient was 0.08 m^{-1} so the minimum value of the reduced scattering coefficient has to be 0.8 m^{-1}. The anisotropy factor is considered to be 0.9, so the minimum value of the scattering coefficient has to be 8 m^{-1}. In order to prove that if the condition isn't fulfilled, we also will consider the case of $\mu_s = 7m^{-1}$ and see if there's a big error that induces us to follow strictly the condition. So, the scattering conditions will go from $7m^{-1}$ to $14m^{-1}$.

Remember that the photon fluence rate in a homogeneous, infinite turbid media is characterized by equation **(24)**. In order to calculate the photon diffusion coefficient, we need to know the speed of the light in water, this is easily calculated by v=c/n, where *n* is the refraction index in this medium. In the case of water, n=1.333.

The fact that the photon fluence rate has a dependence on e^{-r^2} gives it a spherical form, where the peak will be always centered in the direction of the propagation.

In our program, the target will be divided into an array of 51x51 pixels, each one with 0.25x0.25m. This means that the field of view of the system will be 12.5x12.5m. The central pixel will be the closest one to the pulsed source, and we calculate the distance of each pixel by: $r = \sqrt{x^2 + y^2 + z^2}$, where in this case z=20m is the distance between the source and the central pixel of the target.

The illumination on the target at different times is shown in the pictures below.
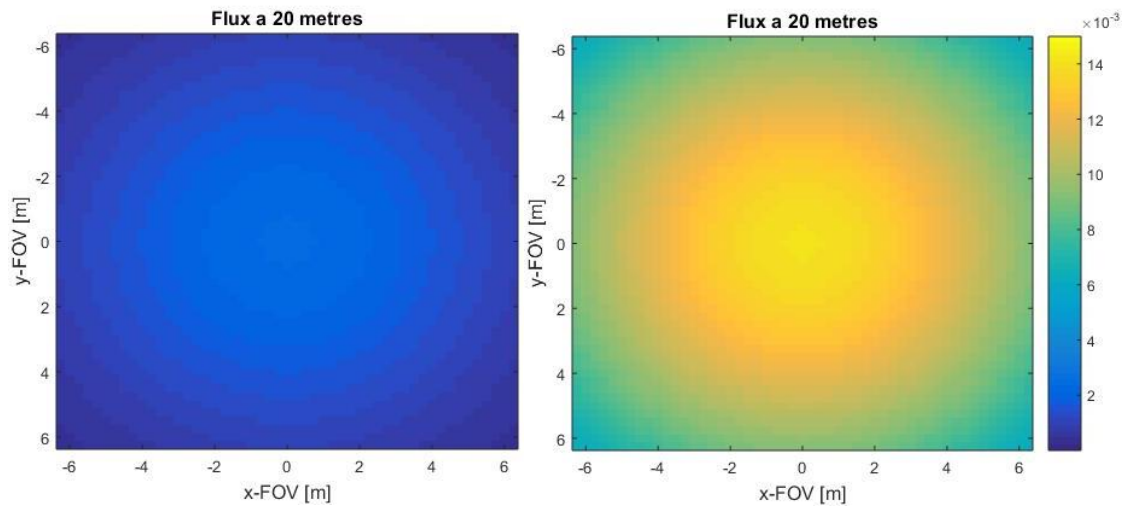
Figure 11. Examples of the illumination on the target at two different times, the left one corresponding to a short t, and the right one corresponding to the time where the maximum fluence rate is found.

As you can see in Figure **11**, the center of the target is always more illuminated than the corners, that is because the distance *r* is lower, proving that the plot in Figure **7** was right.

However, we want to plot this fluence rate as a function of the time, as in Figure **7**, in order to see the differences in it caused by the scattering coefficient.

In Figure **12**, the different photon fluence rate is plotted for the different scattering coefficients. In the legend placed on the top right corner you'll see the values of the scattering coefficient of each function, expressed in m^{-1}.
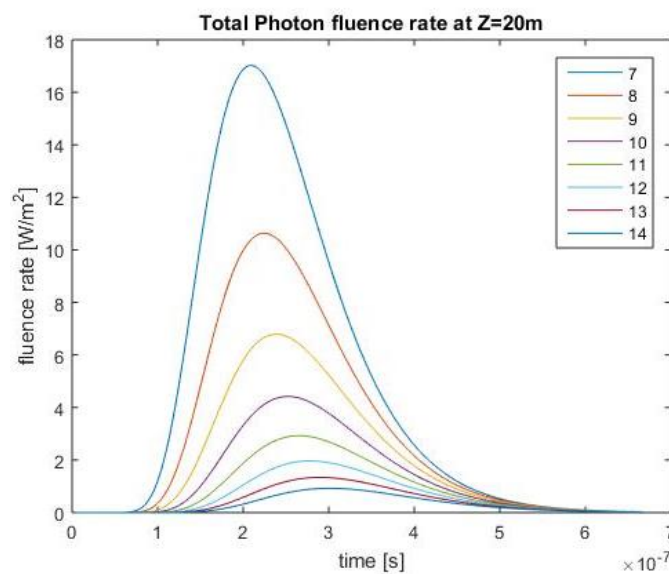
Figure 12. Total photon fluence rate on the target placed at Z=20m, for different scattering coefficients. This fluence rate is the sum of all the segments of the target.

This is the total photon fluence rate for the entire field of view of the system, which means that it is for 12.5x12.5m².

It seems that the peak of the photon fluence rate for each scattering coefficient decays with more or less an exponential form as the scattering coefficient increases. As an example, by doubling the scattering coefficient, the total photon fluence rate has decreased by a factor of 10.

This decrease is easily explained by the definition of scattering. The greater it is; the more scattering events will take place. This means that it is easily to a photon to change the direction and get out of the path and the field of view or to be absorbed before arriving to the target.

Moreover, taking a quick look at Figure 12, it seems that the peak appears later as the scattering coefficient increases. In order to clarify the time of the maximum fluence rate and its value, we make a delta distribution, which is all zero except the time of the peak, with its real value. These functions are plotted in Figure 13.
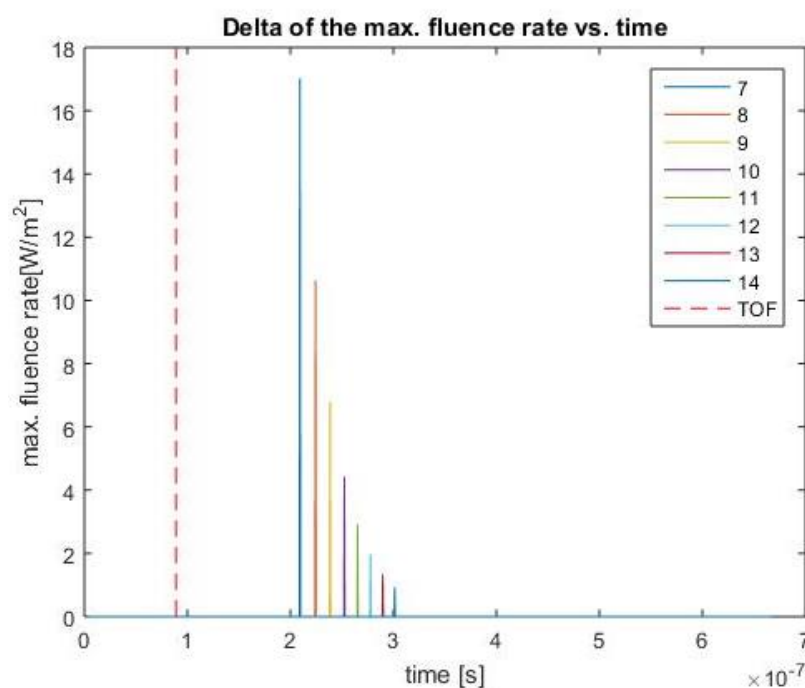
Figure 13. Time where the maximum photon fluence rate takes place, with its value, as a function of the scattering coefficient.

Here, in Figure 13, the delay of the peak as the scattering increases is clearly observed, as well as the same decrease in the maximum value. There's also a red dashed line, which is the time that takes the light to travel 20 meters applying the TOF method. This method,

which is the simplest one, says that this time is $t = {x}/{v}$, where v is the speed of light in the medium of propagation: $v = c/n$, being *n* the refraction index of the medium. So, applying $t = {x \times n}/{c}$, we obtain the time of the red dashed line.

Focusing on the delay, there are two topics to talk about. One is the huge difference between the TOF time and the measured times, and the other one is the comparison between the times applying different scattering coefficients.

Starting with the first topic, at first sight it may seem that the results are wrong, because the time of the maximum is always more than twice the TOF time, but we have to take a look on the Diffusion model condition: ${\mu_s(1-g)}/{\mu_a} > 10$. Knowing that the anisotropy factor is 0.9, we obtain that the scattering coefficient must be 100 times greater than the absorption coefficient: $\mu_s > 100\mu_a$. The reciprocal of both scattering and absorption coefficients are the scattering and absorption mean free paths, respectively, this means that: ${1}/{l_s} > {100}/{l_a}$, which finally means: $l_a > 100l_s$. So, the absorption mean free path is 100 times greater than the scattering mean free path, which implies that the second one must be really small. If the scattering free path is small, this means that the photon will change the direction many times, so it will take more time to arrive to the target. This is also the reason why the time increases as the scattering coefficient also does it.

One of the initial goals was to treat scattering conditions in underwater situations in order to apply it in a 3-D LIDAR camera system. Hence, we want to plot the time of the maximum fluence rate as a function of the scattering coefficient. It is observed below in Figure 14.
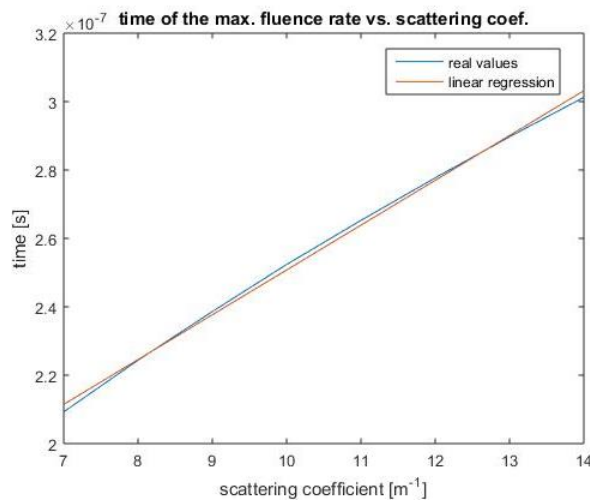

Figure 14. Time when the maximum fluence rate takes place in a target of 12.5x12.5m placed at 20m, as a function of the scattering coefficient of the water. In blue the real values, and in red the first order approximation.

In Figure **14** we see the delay of the peak as a function of the scattering coefficient. One important result is that the obtained times almost follow a straight line, which makes us think in a linear dependence. In order to find which 1ˢᵗ order function fits better the data we have obtained, we make a linear regression (plotted in red), which, as seen in Figure **14**, is very similar to the blue line.

With this linear regression, we obtained that the time of the peak follows the following expression:

$$t_{max} = 1.3103 \times 10^{-8}\mu_s + 1.1975 \times 10^{-7} \ [s] \qquad (29)$$

This expression could be really helpful in order to determinate the scattering coefficient. In this case, this is the expression for a square target of 12.5x12.5 m² and placed at 20 meters. However, we can place a detector in the centre of the target, and make the simulation only for the central pixel. This, will change the relation slightly different, but it will be easier to implement. Recreating these conditions and knowing the time of the maximum fluence rate, we can calculate the scattering coefficient.

Another property that can be measured is the total energy received at a given period of time. For this calculation first we need to remember that the photon fluence rate given by equation **(24)** was expressed in units of $W \, m^{-2}$, which is $J \, m^{-2} s^{-1}$. In order to obtain the energy received in the target, we multiply the photon fluence rate of each pixel with its area (in this case each pixel measures 0.25x0.25m²), and then multiply it by the time interval between one image and another, which is 0.5/v=2.22 ps. The result is shown in Figure **15**.
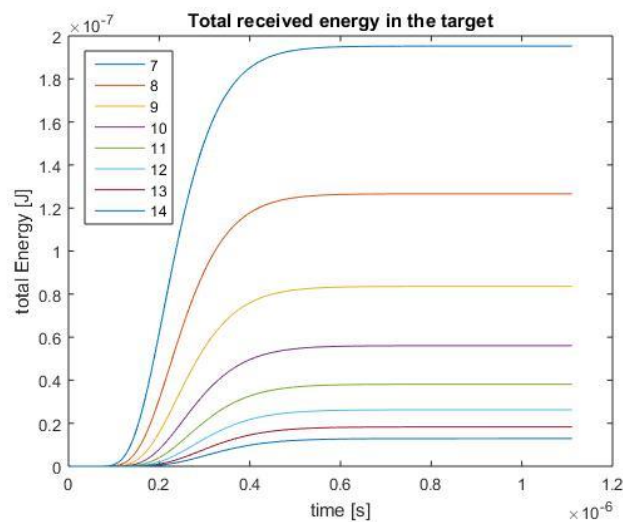

Figure 15. Total received Energy distribution in the target as a function of the time spent.

One fact that need to be remembered is that the total emitted energy was 0.001J, while in all these scattering cases, the maximum total energy is near $2 \times 10^{-7}J$. This means that most part of the energy is not received in the target. This energy loss is due to the spherical behavior of our light source. As it is a point source, the light propagates in every direction, not only in the direction of the target. Moreover, the greater the scattering coefficient is, the lower the total received energy. The reason is that the energy is proportional to the photon fluence rate, so it will have the same properties.

3.1.2.   Variation in the distance to the target

Despite having studied the case of a changing scattering coefficient, the most important aspect in this project is the change in the distance, simulating the goal of a Lidar camera imaging system, which is to calculate the distance to a target by knowing the time light has taken to go to the target and back to a detector.

In order to make a study of the model as a function of the distance to the target, we fix the absorption and scattering coefficients, as well as the anisotropy factor. They are: $\mu_a = 0.07 \ m^{-1}, \mu_s = 8m^{-1} \ and \ g = 0.9$. Moreover, we will consider realistic distances, because light in these media is scattered greatly. This means that we can't consider great distance values, because the fluence rate will be almost negligible. A good range of distances, and the one we will work with, is from 12m to 20m. However, the shape of the photon fluence rate must be similar than the one obtained when changing the scattering coefficient.

In Figure 16, the behavior of the photon fluence rate on a target placed at different distances is shown, and more or less it occurs the same than in the case of the scattering variation. The fluence rate decays exponentially when increasing the distance to the target. If we look close, when increasing the target distance from 12 meters to 20, it decreases by a factor of 100. This is the reason why the fluence rate at higher distances will be really small.
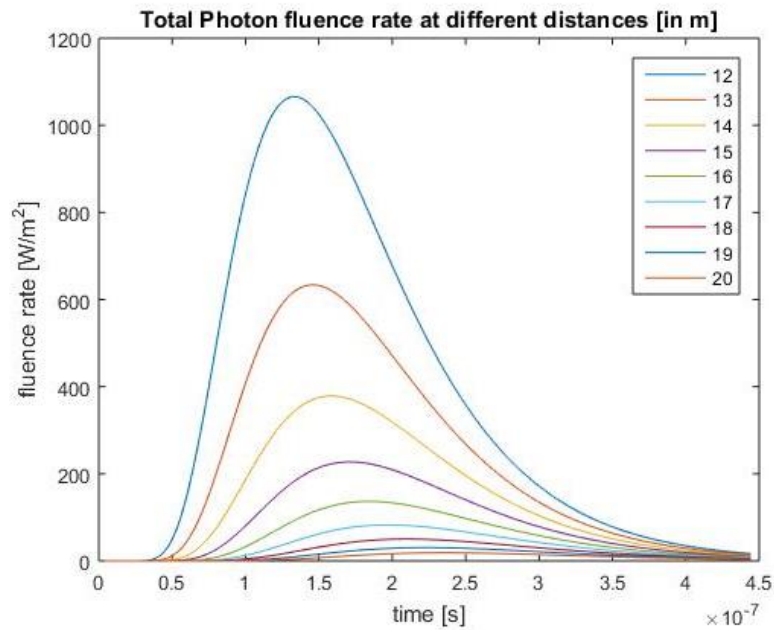
Figure 16. Total fluence rate in the target surface with different target distances, from 12 m to 20 m

However, the value of the peak isn't as relevant as the time it occurs, so, as we made in the "Variation in the scattering Coefficient" chapter before, we make a delta distribution to find out when the peak takes place. This is shown in Figure **17**.
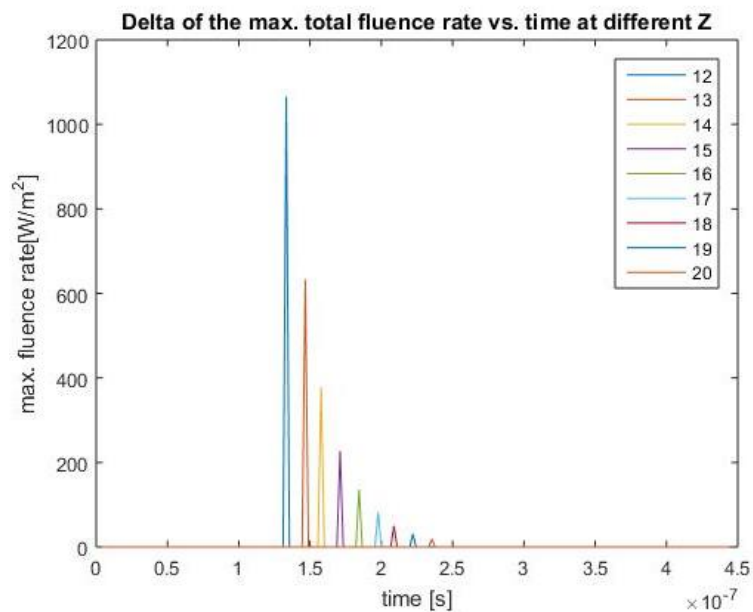
Figure 17. Time where the maximum photon fluence rate takes place, with its value, as a function of the distance to the target.

This time, we don't have a TOF reference line, because as the distance changes, so do the TOF time. Hence, no comparison canbe made. However, what we find in this figure is that it seems that the maximum total fluence rate time follows a straight line.

We want to plot the time of the maximum, but in order to quantify the delay, what is made is to calculate these values of time and then calculate the associated TOF distance by: $dist = v \times t_{max}$. These will give us the relation between the real distance to the target and the one obtained by means of the maximum photon fluence rate. This relation is shown in Figure 18.
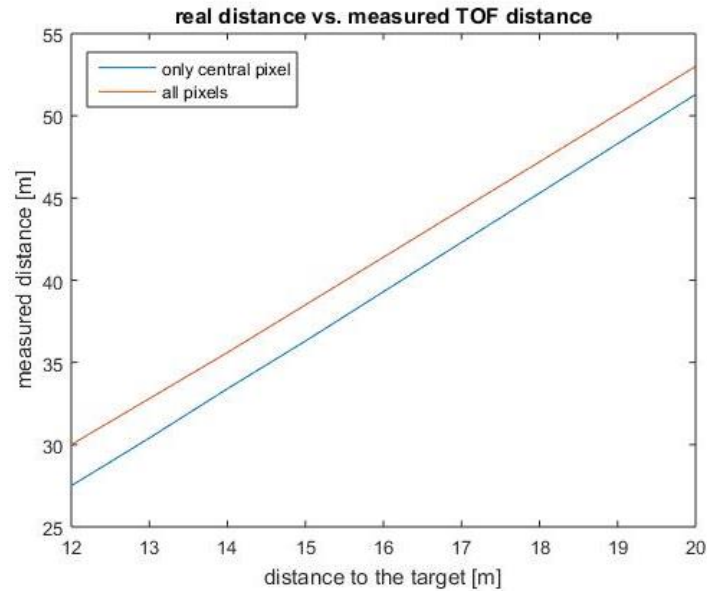
Figure 18. TOF distance calculated by means of the time of the maximum photon fluence rate as a function of the real distance to the target.

Figure 18 confirmed the expectations, the delay produced is linearly dependent on the real distance to the target. What wasn't really expected was the huge delay. Taking an easy value to compare, when the target is placed 12 meters far away from the light source, the time when the maximum fluence rate occurs in the central pixel is equivalent to a distance of 27.5 meters by making $dist = v \times t_{max}$. But if we consider all the target, the time of the peak increases even more. The reason of this extra delay is that for example the surface of the target which is 1 meter far from its centre is greater than the surface of the centre. If the difference between the fluence rate in the centre and in 1 meter far from it isn't too high, the sum of the fluence rate of all pixels placed 1 meter far from the centre is greater than the fluence rate of the centre, giving this extra delay. Moreover, this difference between the time obtained measuring only the central pixel and measuring all of them will be less as the target distance increases. The distance r to each pixel is calculated by: $r = \sqrt{x^2 + y^2 + z^2}$, so if z is big, it will be more relevant than x or y and it will arrive at one point that x and y will be almost negligible and : $r \approx z$. Hence, at a threshold distance to the target, both maximum times will be the same.

We can make a relation between the measured distance and the real distance for the both cases. These are:

For the central pixel:

$$d_{meas} = 2.978d_{real} - 8.038\,[m] \qquad\qquad (30)$$

For all the target:

$$d_{meas} = 2.881d_{real} - 4.673\,[m] \qquad\qquad (31)$$

Equations **(30)** and **(31)** show the relation between the measured distance and its real value. One important aspect is the huge delay, because placing the target one meter further will increase the measured distance almost three meters. Another aspect is that for shorter values of the real distance, this method isn't correct, as it will give a negative measured distance. However, this is not a surprise, as we have seen that the Diffusion Model method fails when the distance to measure is too close to the source.

Despite this method gives us an easy relation between the real distance to the target and its measured value for a good range of values, we will not use it. The reason is that we want to provide help to a 3D LIDAR camera system, and the detector of these cameras doesn't use this technique. Instead of taking the time of the maximum fluence rate value, they take the time when it arrives to a certain threshold value. This method has two main problems. The first one is that the fluence rate decays rapidly when the distance increases, so the depending on the threshold value, the range of measurable distances diminishes.

The other issue could be seen in Figure **16**. Fixing a certain threshold value will add an extra delay to the measure, because the slope of the fluence rate is different for each target distance. Hence, this time we won't have a first order relation between the real distance and the measured, which will make it more difficult to implement.

In order to see clearly the issues of the threshold method, we take three values, one low, another high and the last one medium. The chosen values are $30\,Wm^{-2}, 200\,Wm^{-2}$ and $600\,Wm^{-2}$. The result is shown in Figure **19**
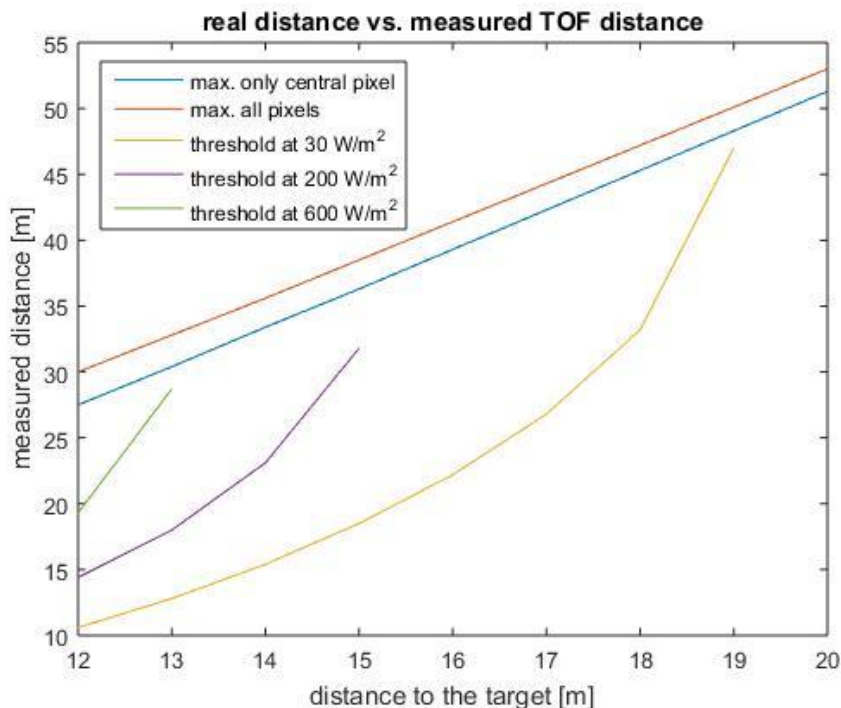
Figure 19. Comparison between TOF distance calculated by means of the time of the maximum photon fluence rate and the one calculated with the threshold technique.

In Figure [19], the extra delay is clearly seen. As the distance to the target increases, so do the delay, making it impossible to make a linear relation between the measured distance and its real value. Looking to the graph, another issue is found: if the value of the threshold is too low, this method will be inaccurate. This is what happens in our case with the threshold value at 30 W/m^2. When the distance to the target is small, we found that the measured distance is lower than its real value, which is wrong because this means that light has travel faster than its speed. An example is found when the real distance is 12 metres. In this case, the measured distance is more or less 10 metres. This is due to the value of the threshold, because it is much lower than the value of the maximum value, causing a great error.

3.1.3.   Validation with TracePro

The key of this project is to characterize the delay of the light in media where scattering is dominant, which is crucial in order to make a 3D Lidar Imaging camera system. However, it is difficult to validate the model with an experiment. The reason is the difficulty to make a medium with the desired scattering coefficient and anisotropy factor. As explained, these

two values, especially the last one, are extremely difficult to measure, because they have big spatial variations.

Therefore, we use TracePro, which is an optical engineering software program for designing and analysing optical and illumination systems. It simulates the movement of the rays in different conditions, drawing them and measuring different properties, such as the flux or the irradiance.

However, TracePro has a big issue, it doesn't have a temporal characterization, which means that we can't validate the delay of the light obtained with the Diffusion Model. Nevertheless, other properties can be measured and validated, such as the flux.

TracePro also uses the Monte Carlo method in order to simulate the movement of the rays, so this chapter will also help to compare the precision of the Diffusion model with the Monte Carlo one in different distances and with different number of rays.

In order to apply the different ocean conditions, a big surface (a cube or a sphere) is needed, simulating the ocean. The reason of this cube is that with TracePro you can't define scattering properties without any solid. In this case, a cube of 1000 metres is generated, which has the desired material and bulk scatter properties:$n = 1.333$, $\mu_a = 0.08 m^{-1}$, $g = 0.9$ and $\mu_s = 8 m^{-1}$.

The source is spherical, assuring that the rays will go to all directions. The radius of this sphere is 5mm and it is placed inside the cube, just in the origin. According to the MATLAB simulation, the energy that emits is 0.00001J, and the laser pulse lasts 0.2 nanoseconds. This means that the initial power is 50kW.

And finally a thin block, which makes the function of the target, is located at different distances. As we are only considering the illumination on the target, and not the returned flux, we consider the target a perfect absorber. The reason is that a ray could arrive to the target by means of one surface, and then get out by means of another. As we only want to count the ray once, and considering a target a solid block, it will be a perfect absorber.

An example of the system is shown in Figure **20**, with the source emitting 200 rays.
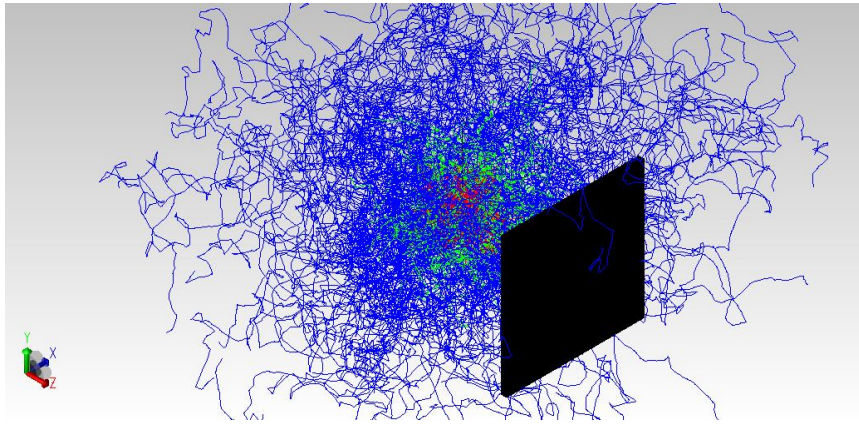
Figure 20. Example of the generated system, with a target placed 10 metres far from the source, which emits 200 rays.

Having a quick look to Figure **20**, we observe that with only 200 rays, almost any ray arrives to the target, even if the target is placed at 10 metres, which is the closest distance me are measuring. We will see later on that this problem disappears by adding more rays.

This chapter will be divided into three subchapters, each one corresponding to a different target distance: 10 metres, 15 and 20.

TracePro generates the random motion by means of a random seed. This means that with the same random seed, photons will appear in the same direction. Therefore, in order to obtain a more accurate value of the flux, several program runs are made, with different values of the seed. Then we will make the mean value of all the results obtained.

Z=10m

Here we will compare the values of the total power absorbed in the target, and its irradiance map, obtained with our simulation in MATLAB and the one given in TracePro for different number of rays. Table **1** shows the result of our simulation.

Total rays	Mean Absorbed rays in target.	Mean Absorbed power [W]	MATLAB power [W]	Mean Absolute error	Mean Relative error (%)
100	10	273.959	281.602	7.643	2.714
500	49.6	272.514	281.602	9.088	3.227
1000	99.1	271.402	281.602	10.199	3.622
2000	195.8	267.864	281.602	13.738	4.878
5000	492.9	268.878	281.602	12.724	4.518
10000	994	268.266	281.602	13.335	4.735
20000	2003.6	267.223	281.602	14.379	5.106
50000	4937.6	265.886	281.602	15.715	5.580

Table 1. Comparison between the flux absorbed by the target in TracePro and in Matlab, with different number of emitted rays.

This is the result of a series of simulations. In the case of 100, 500, 1000, 2000 and 5000 rays, we have made 10 different simulations, each one with a different random seed. With 10000 rays, we have made 8 simulations and with 20000 and 50000 rays, only 5 simulations. The reason of this decrease is that the total computational time increased too much. Just as an example, my laptop only reached 10000 rays, increasing too much this value resulted in a program crash. In the PC of CD6, the system supported as long as 100000 rays, but its computational time was too high. At 50000 rays the deviation of each value of the absorbed flux and its mean value was relatively small, so we decided to stop measuring at that point.

In this distance we see that the method has a little error. When the number of rays is small, the error is also smaller, but that's only a coincidence. With a small number of rays, each one will have a large portion of the emitted power. Therefore, the presence of an extra ray arriving to the target, will variate greatly the quantity of absorbed power, making it an imprecise result. This error disappears when the number of rays is large, as the presence, or the absence, of an extra ray don't affect that much to the final value. The result of this table, as well as the standard deviation obtained with the different measures are shown in Figure , in which is clearly seen the increase of the precision with high number of rays. However, as it increases the precision, the accuracy decreases a little bit, with its mean value more deviated with respect to the Power obtained with the Matlab Simulation. As the number of rays selected doesn't follow a linear relation, we express the graph in a semi-logarithmic way.
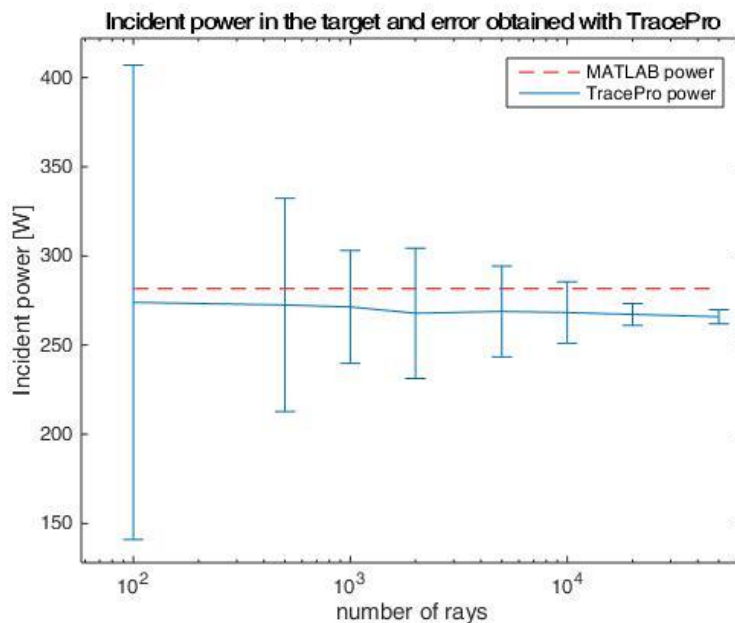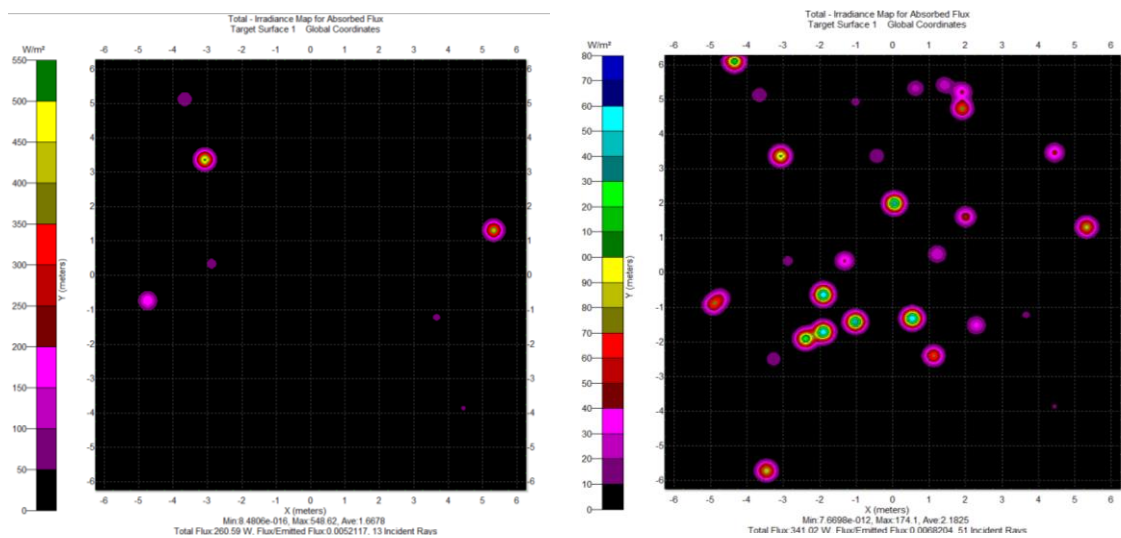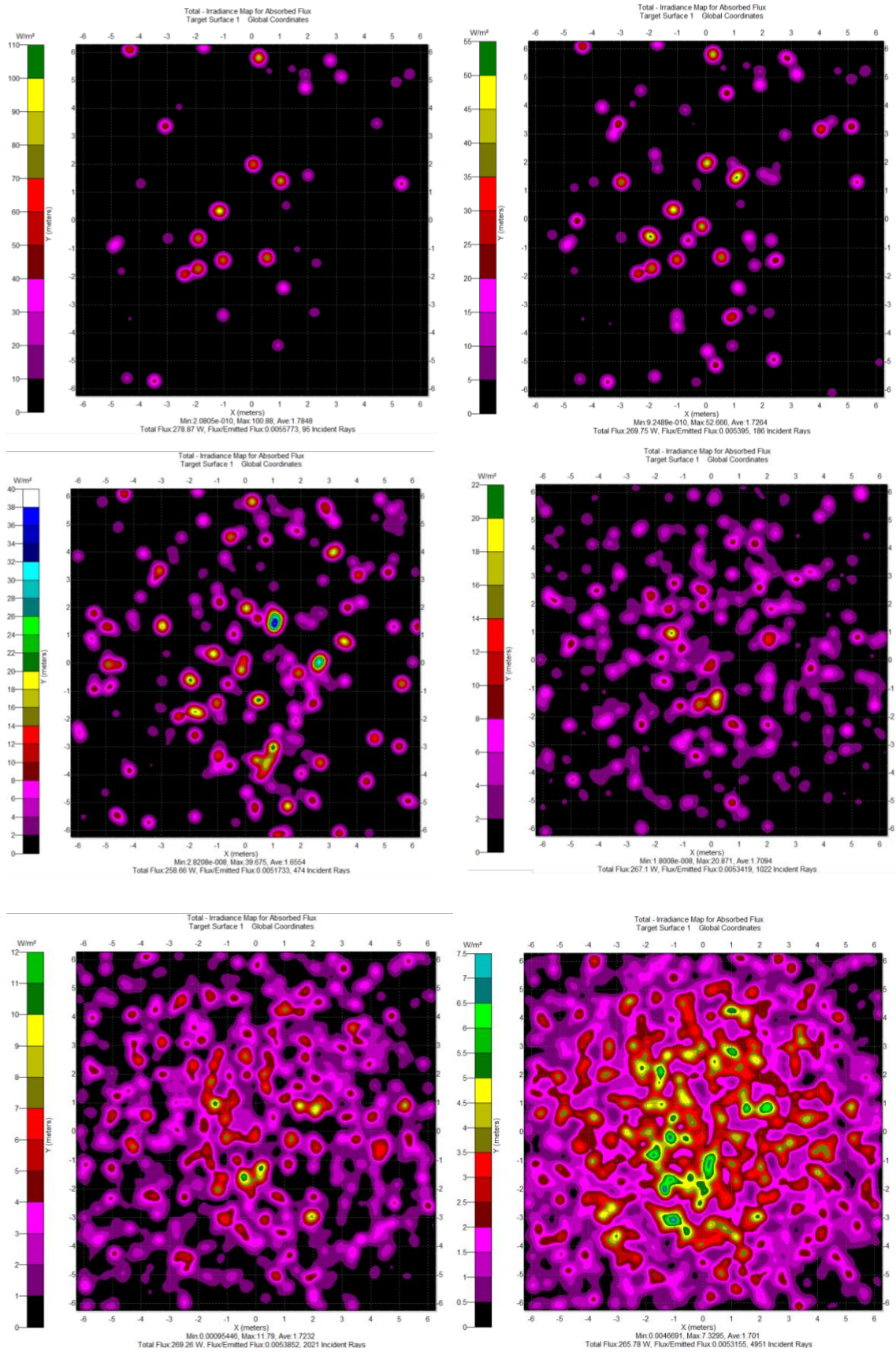
Figure 21.Comparison of the power obtained with TracePro, and its standard deviation, with the simulation power for z=10m

Looking at Figure **22**, this imprecision is easily understood. This figure shows the irradiance map on the target for the incident (and absorbed) flux, for different values of the number of rays.
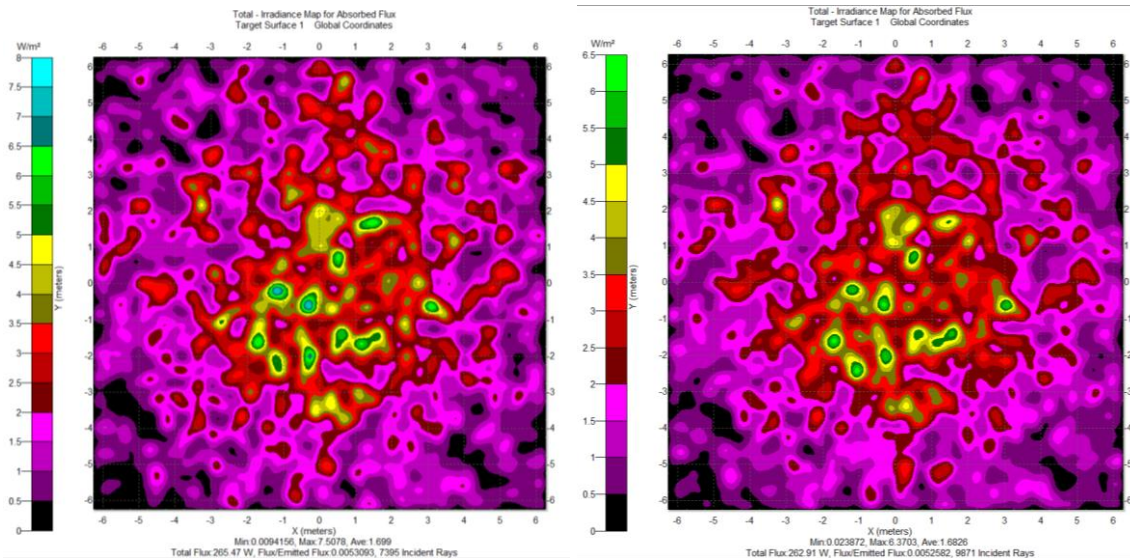
Figure 22. Comparison of the irradiance map on the target with the source emitting a different number of rays. From left to right, (A) 100 rays, (B) 500 rays, (C) 1000 rays, (D) 2000 rays, (E) 5000 rays, (F) 10000 rays, (G) 20000 rays, (H) 50000 rays, (I) 75000 rays and (J) 100000 rays.

There are many features to explain in this group of pictures. The first one was briefly commented above, with a low number of rays, each one contains a great portion of the initial power. As the number of rays increases, the power/ray ratio decrease. This is the reason why the scale that one sees on the left of each picture has each time a lower maximum value.

We also observe that with a lower number of rays, the irradiance map on the target doesn't have any particular shape, there are only a few rays that arrives to the target, in random positions. However, as the number of rays increases, the irradiance map begins to have a spherical shape. With 20000 rays we start to observe that they arrive more rays in the centre of the target than in the corners; situation that become even more visible with larger number of rays, such as 75000 or 100000. This spherical shape coincides with the one we have developed in our MATLAB simulation, and shown in Figure 11, proving that in a big scale, the Diffusion model is a good approximation of the photon transport.

Z=15m

When the target is placed at 15 metres far from the source, the same table stays this time as:

Total rays	Mean Absorbed rays in target.	Mean Absorbed power [W]	MATLAB power [W]	Mean Absolute error	Mean Relative error (%)
100	2.6	33.928	22.836	11.091	48.568
500	13.3	28.727	22.836	5.890	25.792
1000	27.4	25.786	22.836	2.950	12.917
2000	52.6	25.931	22.836	3.095	13.553
5000	132.8	23.442	22.836	0.605	2.649
10000	259.25	23.417	22.836	0.580	2.542
20000	526.2	23.012	22.836	0.175	0.768
50000	1289.4	22.622	22.836	0.214	0.938

Table 2. Comparison between the flux absorbed by the target in TracePro and in Matlab, with different number of emitted rays.

This time the mean absorbed power converges to the value obtained in our MATLAB simulation. With only 100 rays the relative error is almost 50%, exceeding any value that could be coherent. However, this error is becoming smaller as the number of rays increases. The deviation between the mean value and the ones obtained in each sample was also smaller when the number of rays is high, due to what was explained in the case of 10 metres: the ratio power/ray is smaller and therefore the simulation is more accurate. With 20000 and 50000 rays the error was less than 1%, obtaining a more than acceptable error. Another feature that can be observed in Table 2 is that the ratio between the total rays and the mean number of absorbed rays in the target remains constant.

This time the incident power obtained with TracePro converges to the Matlab value, gaining precision as well and accuracy by increasing the number of rays, shown in Figure 23.
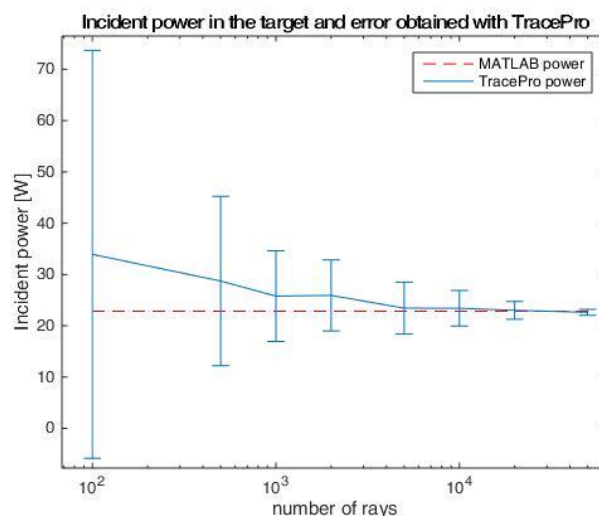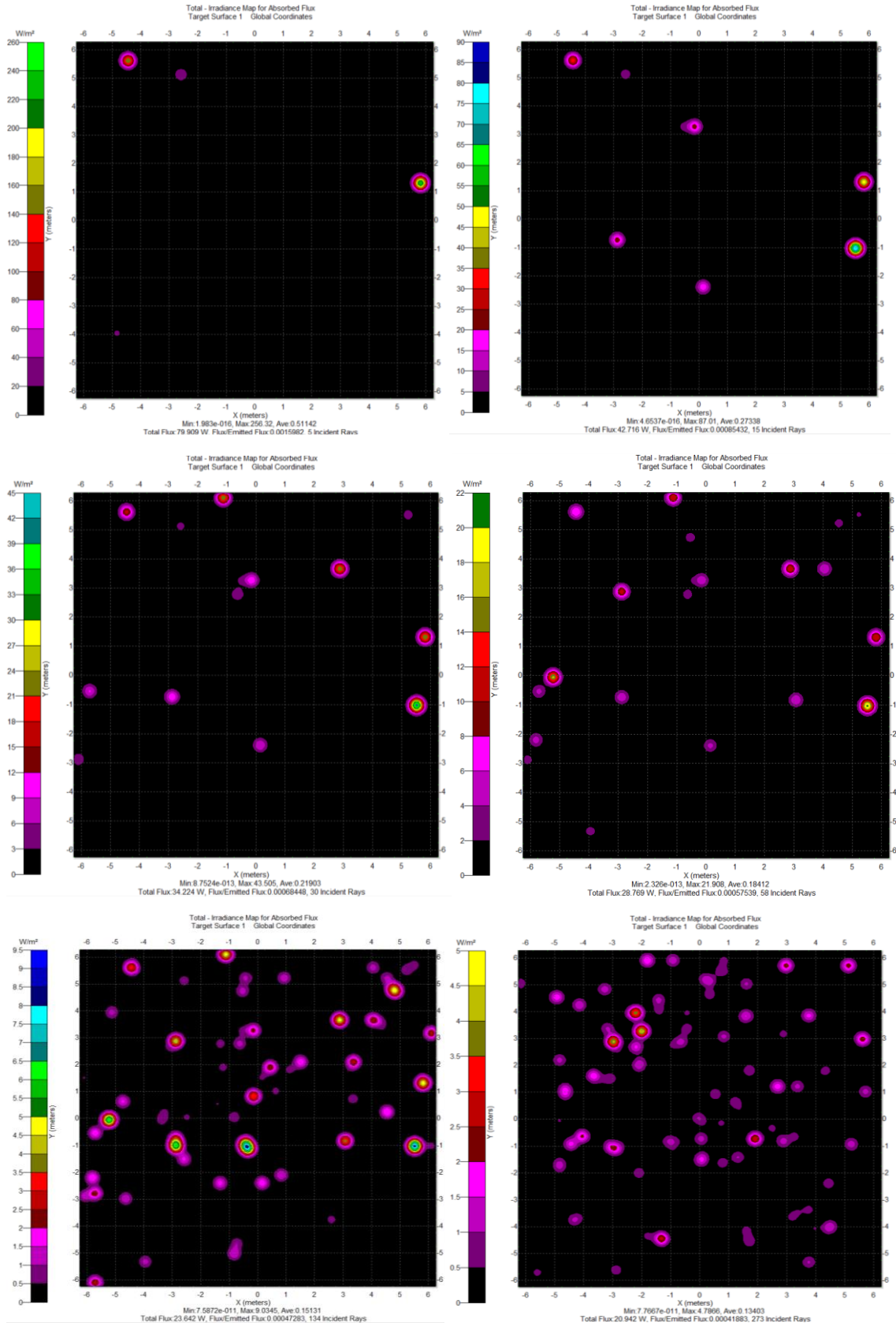

Figure 23. Comparison of the TracePro power, and its standard deviation, with the simulation power for z=15m

Moreover, as we made before, we want to study the location of the incident rays in the target, looking if the same spherical shape that occurred when Z=10, remains at Z=15m. This is shown in Figure **24**.
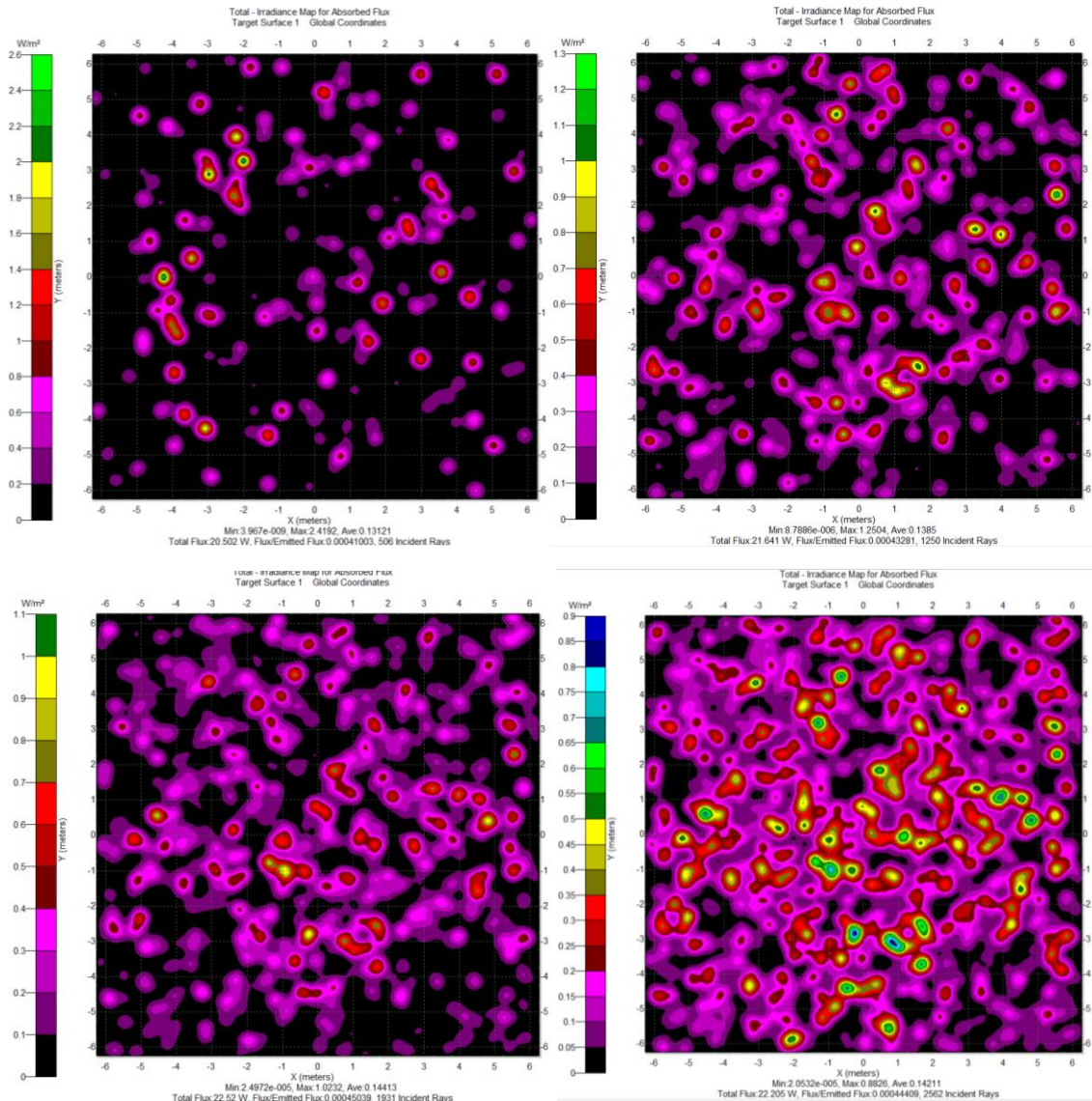
Figure 24. Comparison of the irradiance map on the target with the source emitting a different number of rays. From left to right, (A) 100 rays, (B) 500 rays, (C) 1000 rays, (D) 2000 rays, (E) 5000 rays, (F) 10000 rays, (G) 20000 rays, (H) 50000 rays, (I) 75000 rays and (J) 100000 rays.

If we make a comparison between Figure 24 and the same group of pictures, but obtained when the distance between the source and the target is 10 metres (Figure 22), we observe that with a few rays, there's no difference. In both cases, they arrive only a small portion, which are incident in random positions. Differences appear when the number of emitted rays is high, such as 75000 or 100000 rays. In Figure 22 we clearly saw a circle, where the flux was greater than in the corners. Nonetheless, in Figure 24 this circle is more difficult to be appreciated. That's because the distance to the target is greater, which means that less rays will arrive to the target, and the ones who make it, will arrive more disperse. This is also the reason why there are small zones in the surface without any incident ray.

Z=20m

Total rays	Mean Absorbed rays in target	Mean Absorbed power [W]	MATLAB power [W]	Mean Absolute error	Mean Relative error (%)
100	0.1	1.511	1.905	0.393	20.675
500	2.3	2.290	1.905	0.384	20.197
1000	5.2	2.091	1.905	0.186	9.788
2000	10.4	2.017	1.905	0.112	5.887
5000	25.1	1.772	1.905	0.132	6.955
10000	50.12	1.899	1.905	0.005	0.305
20000	102.6	1.842	1.905	0.063	3.316
50000	247.8	1.940	1.905	0.035	1.844

Table 3. Comparison between the flux absorbed by the target in TracePro and in Matlab, with different number of emitted rays.

When the distance between the source and the centre of the target is 20 metres, we found that with our MATLAB simulation, the total power of the incident rays decreased by a factor of ~10 from the value obtained with Z=15, being 1.90520W. Considering the initial power, which was 50000 W and the fact that it is only measuring the power on the target, we can consider this distance too far from the source, because the total reflected power on the detector would be too small. Another fact that makes us think that 20 metres is not an appropriate distance is that only a few rays arrive to the target. As an example, we made 10 times the simulation with 100 rays, and only in one sample a ray arrived to the target. This problem could also be seen with the ratio incident (or absorbed) rays/total emitted rays, which remains almost constant at 0.005 (a 0.5%).

Despite the fact that it couldn't be an appropriate distance, the error obtained in the measurement of the absorbed power is relatively small when lots of rays are emitted, already explained. From 10000 rays the error is less than a 5% of the MATLAB power. This is graphically shown in Figure 25.
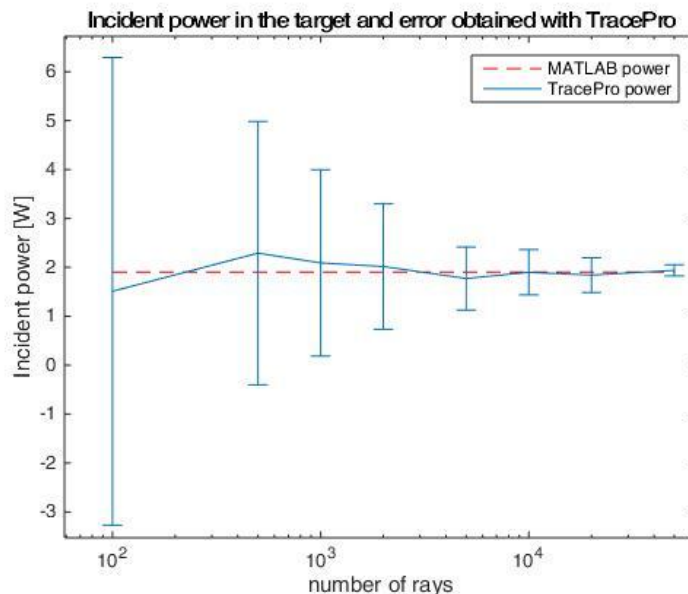
Figure 25. Comparison of the power obtained with TracePro, and its standard deviation, with the simulation power for z=20m

However, this time there won't be the pictures of the irradiance map, as the number of rays that arrive to the target were so small that didn't show anything relevant.

3.2. Illumination of the detector: implementation and validation

Once the light arrives to the target, we have to think about the return flux. In our case, we consider a detector, which is placed next to the source, with a neglectful distance to it. Hence, the distance between each segment of the target and the source is the same that to the detector. We also consider the detector as small as a point.

The target has a reflectivity coefficient, that would depend on its material. In our case, the reflectivity of the target is 0.18. This reflectivity is multiplied by the Incident flux to obtain the reflected flux. Once we have made it, we consider each segment of the target an independent light source. So, considering that the target is divided into 51x51 segments, in the return flux we will have 2601 sources. And here is the main issue of the returned flux: it depends on 4 variables. Two of them are x and y, which will give us the location of the target

segment, and, therefore, this will help us to classify the different light sources. Another variable will be the time of the returned pulse. However, we have to add the time of the initial pulse, as the value of S_0 is not constant now, because it depends on the flux that arrives to the target at different times.

In order to convert this 4D problem into a 3D we make an array of time values, which will be the different moments of time in which the detector will measure the flux. This time array will be the same than the initial time array.

We apply Equation **(24)** for each segment of the target first (x,y), and then for each value of the initial time. Considering the values of the returned time array as t, for tk=1: length (initial time), we will have S_0 (x,y,tk) instead of always the same S_0. For each initial time value, we will have an array of values of the returned flux on the detector. Then we sum the initial time tk with every value of the return time array, obtaining the total time. We repeat it for all the values of the initial time array. The result is that, for each segment of the target, or in other words, for each point source, there are two big vectors: one for the total time and one for the returned flux.

This method has one problem: if the length of the initial time vector is t_1, the value of the position t_1+1 of the total time vector will be less than the position t_1. Making an easy example, if both times go from 1 to 5, the total time array will be [2 3 4 5 6 3 4 5 6 7 4 5 6 7 8 5…], because the first five values correspond to the initial time 1, the second five values to the initial time 2 etc. However, we know the minimum value of the total time, its maximum and its time step. In the example, the minimum is 2 (1+1), the maximum 10 (5+5) and the time step 1, corresponding to the time step of both initial and return time arrays. So, we can make a total time array without repetitions:

```
time=min(t_tot_vec):t_tot_vec(2)-t_tot_vec(1):max(t_tot_vec)
```

But now, how can we order the values of the return flux array in order to coincide to its total time?

First, we create a square matrix with the same dimension of the length of the total time array, being all the values zero. The aim of this matrix is to put all the values of the flux that have the same total time together. That's why each column of the square matrix will correspond to a certain value of time: the first column will correspond to the minimum time and the last one to the maximum. And how many combinations we have with the minimum

value? Only one, the one with the first value of both the initial and the return time. So in the first column there will be only one value different from zero and it will be the position (1,1). In the first row there will be the values corresponding of the first value of the initial time (in our example, the first 5 values). In the second row, the ones with the second value of the initial time (the second 5 values) … We have that all the positions below the diagonal of the matrix will be zero. In the case of our 5x5 example, the matrix will have the following shape:

$$
\begin{matrix}
A & B & C & D & E & 0 & 0 & 0 & 0 \\
0 & F & G & H & I & J & 0 & 0 & 0 \\
0 & 0 & K & L & M & N & P & 0 & 0 \\
0 & 0 & 0 & Q & R & S & T & U & 0 \\
0 & 0 & 0 & 0 & V & W & X & Y & Z \\
 & & & & \vdots & & & & \\
0 & 0 & 0 & 0 & 0 & 0 & 0 & 0 & 0
\end{matrix}
$$

And then all we have to do is to sum all the values of each column to have the total flux for each total time, converting this problem from 4D to 3D.

This isn't a fast method, as there are many loops in the program, so, the computational time of the program increased considerably by adding this return illumination. However, we were able to obtain certain results, as in the chapter before, when changing the scattering coefficient and when changing the distance to the target. These results are explained just below.

3.2.1. Variation in the scattering coefficient

Using the same properties than the ones of the "Illumination on the target" chapter, we have obtained the following results:
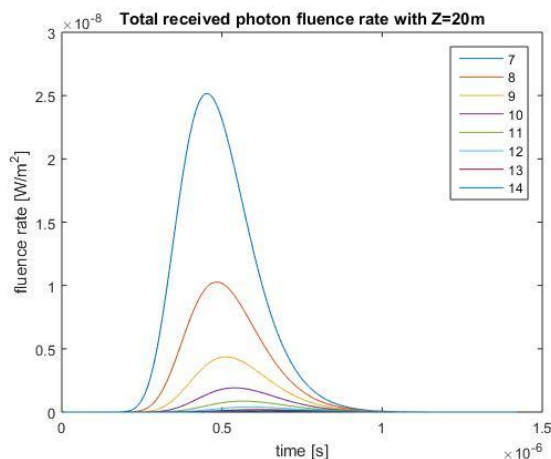

Figure 26. Photon fluence rate on the detector when the target is placed at Z=20m, for different scattering coefficients.

The first difference we see between the illumination on the target (Figure 12) and on the detector, is the value of the obtained peaks. While on the target the maximum values of total photon fluence rate stayed between 1 and 18 W/m², on the detector the fluence rate is considerably less. Between 10^{-9} and $2.5 \times 10^{-8} \text{W/m}^2$. One of the reasons is that the surface of the detector is smaller than the target's surface, so considering almost a point, it is much more improbable that a photon arrives to the detector. The other reason is that as the distance increase, so do the dispersion.

Moreover, the difference between maximum values are greater, as, for example, in Figure 26 there are only 5 visible lines out of the 8 that are drawn, instead of the 8 that were visible in Figure 12.

Now we want to see if the distance measured is similar to the measurement obtained in the target. The biggest approximation could consider that the time of the maximum in the detector would be twice the time in the target. We want to look if it is true or not.
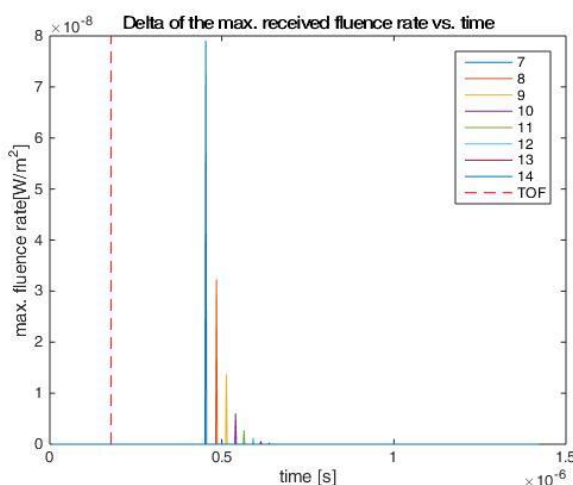

Figure 27. Time where the maximum photon fluence rate at the detector takes place, with its value, as a function of the scattering coefficient.

In Figure 27, the time when the maximum value takes place stays always near 0.5×10^{-6} or 5×10^{-7} for all the scattering coefficients and in the target, the range was $2 - 3 \times 10^{-7}$, so it is approximately twice the time obtained in the target. Moreover, the first of these times, corresponding to $\mu_s = 7m^{-1}$, is a little bit more than twice the TOF time in both cases.

We convert this time into distance, by d=v/2t, where this 2 states that light has travel twice the distance (to the target and come back), and this is the result:
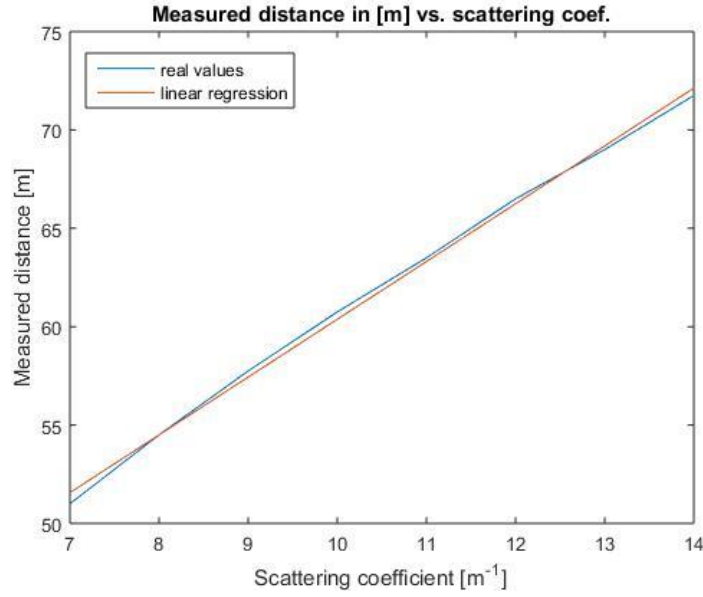
Figure 28. Distance obtained by means of d=v/2t, being t the time when the maximum fluence rate takes place in the detector, as a function of the scattering coefficient of the water. In blue the real values, and in red the first order approximation.

The obtained distances also follow almost a straight line, so a linear regression is made, the result of this regression gives us a first order relation:

$$d = 2.935\mu_s + 31 \ [m] \qquad (32)$$

Which in terms of time, stays as:

$$t_{max} = 2.6104 \times 10^{-8}\mu_s + 2.75486 \times 10^{-7} \ [s] \qquad (33)$$

Being a very similar relation with the one obtained in the target (Equation **(29)**).

3.2.2. Variation in the distance to the target

This time we also keep the properties of the "Illumination on the target" chapter, which were: $\mu_a = 0.07 \ m^{-1}, \mu_s = 8m^{-1} \ and \ g = 0.9$ and also the same measurable distances, from 12m to 20m

In Figure **29**, the behavior of the photon fluence rate on the detector, when the target is placed at different distances, is shown. The fluence rate decays exponentially when increasing the distance to the target and it seems that, as happens with varying the scattering

coefficient, this decay is greater in the target. Making a comparison with the photon fluence rate in the target (Figure **16**), we observe that it has been reduced by a factor of $\sim 10^6$, due to the reasons already explained before. Also the differences between the maximum fluence rate with different distances have increased.
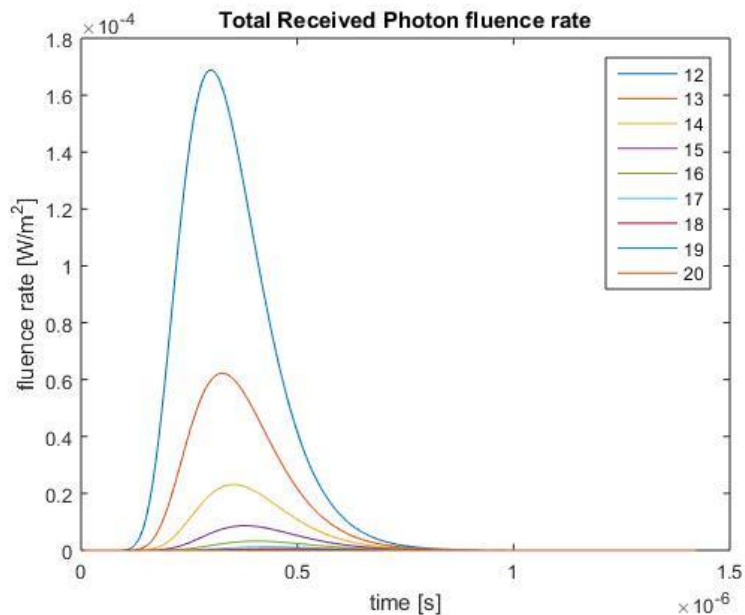

Figure 29 Total fluence rate in the detector with different target distances, from 12 m to 20 m

This difference increase implies that it is more difficult to find a threshold value that fits a good range of distances without adding too much delay to the measure. However, it doesn't affect the time that the maximum value takes place. Hence, the relation between the measured distance and its real value using the time of the maximum should keep on being almost a straight line. This is shown in Figure **30**
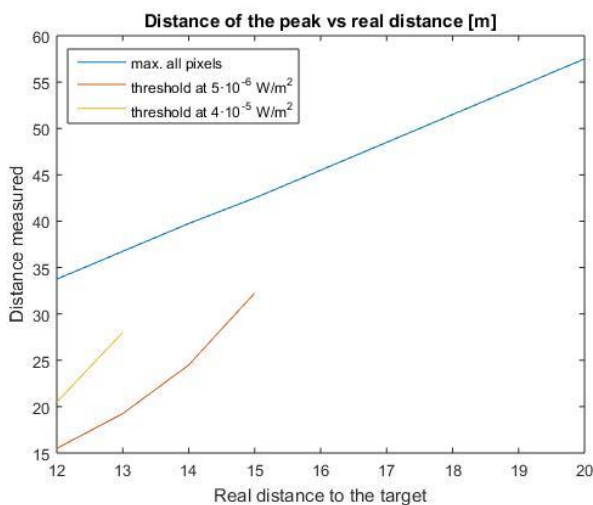

Figure 30. Comparison between TOF distance calculated by means of the time of the maximum photon fluence rate and the one calculated with the threshold technique.

First of all, we observe what was stated before, it is difficult to find a threshold value for all the distances. In this case, the maximum number of measured distances with the lowest threshold value is 4, from 12 to 15 metres.

Talking about the maximum photon fluence rate, its time is almost a straight line, but, compared with the time obtained in the target (Figure **19**), the delay is always a little bit greater. The first order relation between the measured distance and its real value is:

$$d_{meas} = 2.9625 d_{real} - 1.8166 [m] \qquad (34)$$

Very similar to equations **(30)** and **(31)**. The comparison of the obtained distances is made in Table **4**. There, we see that the distance obtained in the detector is always more or less four metres more than the distance obtained only applying the TOF method on the target.

Real distance [m]	12	13	14	15	16	17	18	19	20
Distance measured on target [m]	29.9	32.8	35.6	38.5	41.4	44.3	47.2	50.1	52.9
Distance measured on detector [m]	33.75	36.75	39.75	42.50	45.50	48.50	51.50	54.50	57.50

Table 4. Comparison between the distance obtained by means of the TOF in the target and in the detector.

Chapter 4

Conclusions

In this project we have seen the theoretical part of the Diffusion model, making also a simulation of this method under scattering conditions. All the coefficents used in the project are extracted from different papers, so these conditions could be found in sea water.

We have also made a comparison between the Diffusion model and the Monte Carlo method. The second one gives only an accurate description of the fluence rate when the number of rays is large ($\sim$100000 rays the fluence rate starts to have the proper shape). However, it is very cost-effective, taking too much time to make the simulation. Due to this large computation time and the fact that the high spatial resolution of the Monte Carlo method isn't needed, a simplest and fastest model is required, the Diffusion Model. Applying the diffusion model in strong scattering conditions, we see a huge delay, usually more than twice the time obtained by t=x/v. The reason of this delay is that, photons travel much more distance before arriving to the target.

If we look at equations **(30)**, **(31)** or **(34)**, which give the relation between the real distance to the target and the measured distance in different cases of our simulation, we find that the diffusion Model isn't accurate in short distances. When the target is too close to the source, the relation will give a negative measured distance. So, we have proved that the Diffusion Model is not valid for short distances.

We have also made a simulation with TracePro, under the same conditions of the MATLAB code, and we have seen that the rays don't travel higher distances. As they change the direction multiple times, hardly ever a ray arrives to a target placed at distances such as 40 or 50 metres, which means that the range of distances is limited.

I hope this project has helped to the development of a multihit LADAR imaging camera system, which is already under construction in CD6. The aim of this camera is to work under diffusion conditions such as turbid water or fog, making it a state-of-art camera in the field of the LIDAR cameras.

Chapter 5

Bibliography

[1] B. Hagenbeuker; "A 3D time of flight camera for object detection" (2007)

[2] R.D. Richmond and S.C. Cain; *Direct Detection LADAR systems. (2010)*

[3] S. Royo et al.; "Metrología de objetos extensos en el CD6: Reconstrucción estereoscópica e imagen LIDAR." *e-medida. Revista Española de Metrología, nº 9.* (2015)

[4] Ocean Optics Web Book; URL: *http://www.oceanopticsbook.info/*

[5] Richard B. Miles, Walter R. Lempert, Joseph N. Forkey; "Laser Rayleigh Scattering". *Measurement science and technology,* **12.** (2001)

[6] David W. Hann; "Light Scattering Theory". (2009)

[7] Kenneth M. Case, Paul Frederick Zweifel; *Linear Transport Theory* (1967)

[8] S. Chandraskkhar; *Radiative Transfer* (1960)

[9] S. L. Jacques and B. W. Pogue; "Tutorial on diffuse light transport" *Journal of Biomedical Optics.* **13**, 041302 (2008)

[10] S. L. Jacques; "Time-resolved reflectance spectroscopy in turbid tissues" *IEEE Transactions on Biomedical Engineering.* **36,** 1155 – 1161 (1989)

[11] T. Durduran et al.; "Diffuse optics for tissue monitoring and tomography" *Reports on Progress in Physics.* **73,** 076701. (2010)

[12] S.L. Jacques; "Monte Carlo Modeling of Light Transport in Tissue" *In Optical-Thermal Responses of Laser-Irradiated Tissue (2009)*

[13] S.A. Prahl et al.; "A Monte Carlo Model of Light Propagation in Tissue" *SPIE Proceedings of Dosimetry of Laser Radiation in Medicine and Biology,* **IS 5**, 102-111 (1989).

[14] C.L. Gallegos et al.; "Modeling spectral diffuse attenuation, absorption, and scattering coefficients in a turbid estuary" *Limnology and Oceanography,* **35,** 1486-1502 (1990)

[15] John T.O. Kirk; "Estimation of the absorption and the scattering coefficients of natural waters by use of underwater irradiance measurements" *Applied Optics,* **33,** 3276-3278 (1994)

[16] M. Babin et al.; "Variations in the light absorption coefficients of phytoplankton, nonalgal particles, and dissolved organic matter in coastal waters around Europe" *Journal of Geophysical Research,* **108** (2003)

[17] K.S. Shifrin; *Physical Optics of Ocean Water* (1988)

[18] W.S. Pegau et al.; "Absorption and attenuation of visible and near-infrared light in water: dependence on temperature and salinity" *Applied Optics,* **36**, 6035-6046 (1997)

[19] D. Sevrain et al.; "Measuring the scattering coefficient of turbid media from two-photon microscopy" *Optics Express,* **21** 25221-25235 (2013)